Head-to-head comparison of lung perfusion with dual-energy CT and SPECT-CT

S. Si-Mohamed, C. Moreau-Triby, P. Tylski, V. Tatard-Leitman, Q. Wdowik, S. Boccalini, R. Dessouky, P. Douek, L. Boussel

Head-to-head comparison of lung perfusion with dual-energy CT and SPECT-CT

Short title

Lung dual-energy CT perfusion imaging

Salim SI-MOHAMED [a,b]*, Caroline MOREAU-TRIBY[c], Perrine TYLSKI[d], Valérie TATARD-LEITMAN[b], Quentin WDOWIK[a], Sara BOCCALINI[a] , Riham DESSOUKY[e], Philippe DOUEK[a,b], Loïc BOUSSEL[a,b],

[a] Department of Radiology, Hospices Civils de Lyon, 69500 Bron, France
[b] Univ Lyon, INSA - Lyon, Université Claude Bernard Lyon 1, UJM-Saint Etienne, CNRS, Inserm, CREATIS UMR 5220, U1206, 69621 Lyon, France
[c] Department of Nuclear Medicine, Hospices Civils de Lyon, 69500 Bron, France
[d] Medical Physics and Radioprotection, Hospices Civils de Lyon, 69500 Bron, France
[e] Department of Radiology, Faculty of Medicine, Zagazig University, 44519 Zagazig, Egypt.

*** Corresponding author**: salim.si-mohamed@chu-lyon.fr

Department of Radiology, CHU Louis Pradel, 59 Boulevard Pinel, 69500 Bron, France

Sources of support that require acknowledgement: This work was not supported by grants.

Conflicts of Interest and Source of Funding: There is no conflict of Interest.

Manuscript type: Original research

CTEPH: chronic thromboembolic pulmonary hypertension

CTDIvol: Volume computed tomography dose index

CZT: Cadmium-Zinc-Telluride

DECT: dual-layer dual energy computed tomography

FEV: Forced expiratory volume

PBV: perfusion blood volume

PE: Pulmonary embolism

99m-Tc: 99m-Technetium

SPECT-CT: scintigraphy photon emission computed tomography-computed tomography

Abstract

PURPOSE. To compare the quantitative and qualitative lung perfusion data acquired with dual energy CT (DECT) to that acquired with a large field-of-view cadmium zinc telluride camera single-photon emission CT coupled to a CT system (SPECT-CT).

MATERIALS AND METHODS. A total of 53 patients who underwent both dual-layer DECT angiography and perfusion SPECT-CT for pulmonary hypertension or pre-operative lobar resection surgery were retrospectively included. There were 30 men and 23 women with a mean age of 65.4 ± 17.5 (SD) years (range: 18-88 years). Relative lobar perfusion was calculated by dividing the amount (of radiotracer or iodinated contrast agent) per lobe by the total amount in both lungs. Linear regression, Bland-Altman analysis, and Pearson's correlation coefficient were also calculated. Kappa test was used to test agreements in morphology and severity of perfusion defects assessed on SPECT-CT and on DECT iodine maps with a one month interval. Wilcoxon rank sum test was used to compare the sharpness of perfusion defects and radiation dose among modalities.

RESULTS. Strong correlations for relative lobar perfusion using linear regression analysis and Pearson's correlation coefficient (r = 0.93) were found. Bland-Altman analysis revealed a -0.10 bias, with limits of agreement between [-6.01; 5.81]. High level of agreement was found for morphology and severity of perfusion defects between modalities (Kappa = 0.84 and 0.86 respectively) and on DECT images among readers (Kappa=0.94 and 0.89 respectively). A significantly sharper delineation of perfusion defects was found on DECT images (P < 0.0001) using a significantly lower equivalent dose of 4.1 ± 2.3 (SD) mSv (range: 1.9-11.85

mSv) compared to an equivalent dose of 5.3 ± 1.1 (SD) mSv (range: 2.8-7.3 mSv) for SPECT-CT, corresponding to a 21.2% dose reduction ($P = 0.0004$).

CONCLUSION. DECT imaging shows strong quantitative correlations and qualitative agreements with SPECT-CT for the evaluation of lung perfusion.

Keywords: Tomography, X-Ray Computed/methods; Lung; Perfusion; Tomography, Emission-Computed, Single-Photon; comparative study

Introduction

Pulmonar ventilation/perfusion scintigraphy and computed tomography (CT) are well-established imaging techniques for the diagnosis of chronic thromboembolic pulmonary hypertension (CTEPH) (1). Both techniques are also required as a part of the diagnostic work up prior to lobe reduction surgery or radiation therapy for lung cancer. Pulmonary scintigraphy as a functional modality is indicated for perfusion defect imaging or relative lobar perfusion to anticipate post-operative lung function (2,3). Then CT as a morphological modality is indicated for pulmonary vessel imaging or resection management before volume reduction surgery (4,5). However, although CT can be used using low dose protocols, concerns remain with regard to this combined approach in terms of radiation exposure, cost-effectiveness, and convenience for patients (6,7).

With the introduction of dual energy CT (DECT) systems, a new type of imaging, that is specific to the iodine content called “iodine map”, has emerged (8). Experimental studies comparing iodine maps to scintigraphy, found that qualitative and quantitative imaging of the lung iodine distribution is a surrogate marker of lung perfusion (9,10). The few studies that have investigated the use of iodine maps defects showed excellent diagnostic performance for the diagnosis of lung perfusion defects in patients with pulmonary embolism (PE) (11–13) and those with CTEPH (14,15). Another study showed high accuracy in measuring the lobar perfusion volume for the prediction of the postoperative lung function compared to multiplanar perfusion scintigraphy using ^{99m}Tc macro aggregated albumin (MAA-Tc^{99m}) [14]. In addition, some studies have compared the performance of iodine maps to that of SPECT (which is the gold standard imaging technique that allows registration at the segmental level) for the diagnosis of perfusion defects (13,16). Initially, these two modalities were compared directly and the sensitivity for perfusion defect of DECT with respect to SPECT varied from

76.7% to 96.0% (13,16). Later on, both modalities were compared to angiography, and 92.0% sensitivity was found for perfusion defect of DECT compared to 85.0% for SPECT (17). However, agreements between DECT and scintigraphy (both multiplanar and SPECT) in the diagnosis of perfusion defects were fair (14,15,18).

The assessment of lung perfusion has been subjected to recent technological developments in nuclear medicine and radiology. First, SPECT-CT hybrid system allows a three-dimensional (3D) perfusion registration and fusion with a low-dose CT for spatial anatomy (19). This new technique has demonstrated greater sensitivity, specificity, reproducibility, and lower indeterminate rate of perfusion defects than planar scintigraphy with stronger correlation with clinical outcome after lobe volume reduction surgery (19–21). In addition, cadmium zinc telluride (CZT) gamma cameras provide greater sharpness, contrast, and quantitative accuracy for ^{99m}Tc by comparison with analog cameras (22,23). Second, DECT systems with dual-layer scintillator detectors do not require acquisition parameter adjustment permitting retrospective reconstruction of a data set for spectral imaging purposes (24); such systems have demonstrated great *in vitro* quantification capabilities for minimal iodine concentrations using low and up to 7 mGy radiation doses (24–26). The third most recent development is in the software for semi-automatic quantification, which allows calculation of relative lobar perfusion. In light of these new developments, a reevaluation of DECT perfusion imaging as a qualitative and quantitative surrogate marker for lung perfusion is needed.

The purpose of this study was to compare the quantitative and qualitative lung perfusion data acquired with a dual-layer DECT to that acquired with a SPECT-CT large field-of-view CZT camera.

Materials and methods

Patients

The study was approved by the institutional review board and informed consent was waived. From May 2017 to September 2018, all patients who underwent both dual layer DECT angiography and SPECT-CT within 6 weeks of each other for the diagnostic work-up of pulmonary hypertension or pre-operative lobar resection surgery were included in this single center, retrospective study. A total of 85 patients were initially retrieved and 32 patients with acute PE were excluded as this diagnosis did not require both examinations. A flowchart of the study inclusion is shown in Figure 1.

The study population included 53 patients (30 men and 23 women) with a mean age of 65.4 ± 17.5 (SD) years (range: 18-88 years).

Dual-energy CT protocol

DECT perfusion was performed using a dual-layer DECT system (iQon®; Philips Healthcare). Lung CT angiography protocol is described in Table 1 [27]. The amount of iodinated contrast material (iomeprol, Iomeron® 400 mg/mL; Bracco Imaging) injected for each patient was calculated based on the time of acquisition for a flow rate of 3.5 mL/s using the following formula:

Volume of contrast agent (mL) = (estimated total time of CT acquisition [sec] + 6) x flow rate [mL/sec]).

The acquisitions were performed from head to feet and scanning was initiated using a bolus-tracking technique with a threshold of 110 Hounsfield units (HU) in the main pulmonary artery. Conventional images, iodine maps and overlay between those two were reconstructed for each patient using Spectral Philips IntelliSpace Portal 9.0 software (Philips Healthcare) (24).

SPECT-CT protocol

SPECT-CT perfusion examination was performed using a SPECT-CT system equipped with large field of view dual head camera with CZT detectors (D670 CZT; GE Healthcare) (Table 1) and wide-energy high-resolution collimators. Patients were injected under the camera in a supine position with a dose of 150 MBq of Technetium99m-labelled macroaggregated albumin (MAA-Tc99m; Pulmocis, Cis bio international). Perfusion and ventilation images were simultaneously acquired after injection and during inhalation of Kr-81m (Kryptoscan®, Mallinckrodt). A spectrometric window of 140 ± 7.5% keV was used for Tc-99m and 190 ± 10.0 % for Kr-81m. Images were reconstructed using an ordered subset estimation maximization algorithm including resolution recovery with 2 iterations, 8 subsets, and Butterworth post-filtering with a 0.6 frequency cutoff. Lung CT at 120 kVp was performed for 3D anatomic reference. Images were reconstructed with an iterative algorithm (ASiR®; GE Healthcare) with a 40% factor (ASIRv40%). Perfusion images and CT images were reconstructed using semi-automatic lung segmentation software (Q.Lung®; GE Healthcare) and stored for quantitative analysis. Overlay between perfusion and CT images was created for the purpose of qualitative analysis.

DECT and SPECT-CT image analysis

Quantitative analysis of tracer distribution

For both modalities, a nuclear physician (R1, CMT with 15 years of experience) specialized in lung imaging and a radiologist (R2, SSM, with 8 years of experience in thoracic imaging) proceeded to segment both lung lobes in consensus using semi-automatic software. COPD was used for conventional DECT images (IntelliSpace Portal) and Q.Lung® for SPECT-CT images. These software allowed manual exclusion of the main pulmonary vessels and adjustments to fissure location and lung borders (**Figure 2**). This segmentation resulted in lobar mask images that were applied on iodine images for DECT and perfusion images for SPECT-CT. On DECT iodine maps, the mean value of iodine concentrations and number of pixels were recorded using the masks. The quantity of iodine within each lobe was then calculated as follows:

Quantity of iodine (mg) = [mean concentration$_{mg/mL}$] × [number of pixels] × [voxel size$_{mm^3}$].

On SPECT-CT images, a similar automatic quantification of radiotracer within each lobe was performed by calculating the number of counts in each lobe using Q.Lung® software. Finally, the relative contribution of each lobe to the lungs was expressed in percentage (%) for both modalities. As the timing of injection can influence lung perfusion, we also recorded the ratio between iodine concentration within the pulmonary artery and the left atrium.

Qualitative analysis of tracer distribution

All images were interpreted on a clinical workstation (Spectral Intellispace Portal 9.0). The nuclear physician was free to adapt the windowing for SPECT-CT imaging. Diagnosis of perfusion defects was made on SPECT-CT overlay images by the nuclear physician (R1), and considered the gold standard. DECT overlay images were then interpreted by both readers (R1, R2) with a one month interval between SPECT-CT and DECT for R1.

Diagnosis of perfusion defect was based on the European Association of Nuclear Medicine (EANM) guidelines (1). The readers rated at a segmental level using the Boyden's nomenclature (28) (*i*), the pattern of perfusion abnormalities if present into two classes: embolic-type, patchy, and (*ii*), the spatial distribution of tracers on the following scale: 1= 0-50%, 2= 50-100%. The readers were then asked to rate the sharpness of the perfusion defect depiction based on an image criteria score used previously (29) (1: visualization just possible, 2: unsharp borders but defect visible, 3: good visualization, well-defined, 4: perfect

delineation, well-defined anatomy). In addition, the radiologist (R2) recorded the presence and severity (rated as moderate or severe) of artifacts on iodine maps considered as partially or totally altering perfusion analysis in the corresponding segments. Only segment with severe artifacts was considered non-diagnostic. Both readers were blinded to patient outcomes.

Radiation dose

The mean equivalent dose was calculated using CTexpo (30) for CT data and using Tc-99m MAA injection (31), without taking into account the ventilation study for SPECT-CT.

Statistical analysis

Statistical analysis was performed using R (R Foundation for Statistical Computing). Quantitative variables were expressed as means ± standard deviations (SD) and ranges. Qualitative variables were expressed as raw numbers, proportions and percentages. Linear regression analysis including slope, offset, R^2, root mean square error (RMSE) and Pearson correlation coefficient (r) using a 95% confidence interval were calculated for relative lobar perfusion values in both DECT and SPECT-CT. Bland-Altman analysis was also performed, and limits of agreement were defined as a mean difference of ± 1.96 SD. Diagnostic performances of DECT iodine maps in the diagnosis of perfusion defects (sensitivity, specificity, accuracy, positive predictive value [PPV], negative predictive value [NPV]) were calculated along with their 95% CI using SPECT-CT images as the standard of reference. Wilcoxon signed-rank test was used to searche for differences in qualitative (sharpness of the perfusion defect) and quantitative (relative lobar perfusion) findings between DECT and SPECT-CT.

Agreement between the diagnostic modalities used by R1 and R2 to diagnose perfusion defects on DECT at a segment level were tested using Cohen's Kappa. Kappa agreements were then characterized according to Landis and Koch criteria as slight (Kappa = 0.00-0.20), fair (Kappa = 0.21-0.40), moderate (Kappa = 0.41-0.60), substantial (Kappa = 0.61-0.80), or almost perfect (Kappa = 0.81-1.00). The proportion of lobes in which there was an absolute difference of less than 5% between DECT and SPECT-CT for relative lobar perfusion measurements as well as the proportion of cases where there was a 10% difference

was calculated. Differences in radiation dose between DECT and SPECT-CT were searched for using Wilcoxon rank sum test. Significance was set at $P < 0.05$.

Results

Patient characteristics

The mean body mass index in the cohort study was 26.1 ± 5.9 (SD) (range: 16.4 - 43.6). A total of 32 patients (32/53; 60.0%) had perfusion defects. Fourteen patients (14/53; 26.4%) patients underwent both examinations on the same day and 24 (24/53; 45.3%) patients underwent DECT examination first. The mean time between DECT and SPECT-CT was 6.4 ± 9.9 (SD) days (range: 0.0 - 40.0 days). A total of 1060 segments were qualitatively analyzed according to the Bowden's classification. On DECT, 1 segment had severe artifacts and 13 segments had moderate artifacts. A total of 265 lobes were quantitative analyzed. All segments and lobes, including those in 40 patients (40/53; 75.0%) where concentration ratio between the pulmonary trunk and the left atrium was greater than 1, were used in the statistical analysis.

Quantitative perfusion analysis

The mean relative lobar perfusion was 20.0 ± 8.1 (SD) % (range: 0 - 40.2%) for iodine maps and 20.1 ± 8.5 (SD) % (range: 0 - 43.0%) for SPECT-CT images ($P = 0.40$). The slope of the linear regression was 0.88, offset was 2.11, R^2 was 0.87, and RMSE was 2.87. Pearson correlation coefficient (r) was 0.93 (95% CI: 0.92 - 0.95) **(Table 2, Figure 3)**. Bland-Altman analysis revealed a bias of -0.10, with 95.0% limits of agreement from -6.0 to 5.8. Similarly, the results of analysis for individual lobes are provided in **Table 2 and Figures 4 and 5**. Pearson correlation coefficient values were ≥ 0.90 except for the middle lobe which was 0.79 (95% CI: 0.66 - 0.87). Bland-Altman analysis showed bias ranging from -1.60 to 1.32 within limits of agreement ranging from -8.15 to 6.93. Furthermore, 88.0% of the absolute differences between DECT and SPECT measurements were less than 5.0% and 99.6% were less than 10.0%.

Qualitative perfusion analysis

On SPECT-CT images, a total of 265 (265/1060; 25.0%) segments had perfusion defects: 179 (179/1060; 16.9%) were of embolic type and 86 (86/1060; 8.1%) were patchy. On DECT

images, a total of 249 (249/1060; 23.5%) segments had perfusion defects: 162 (162/1060; 15.3%) were of embolic type and 85 (85/1060; 8.0%) were patchy. With respect to SPECT-CT as standard of reference, the sensitivity, specificity, PPV, NPV, accuracy for lobar perfusion defects were 89.4% (95% CI: 82.6 - 93.4%), 96.5% (95% CI: 92.1 - 98.5%), 95.6% (95% CI: 90.9 - 97.8%), 91.4% (95% CI: 85.6 - 94.9%) and 93.0% (95% CI: 87.6 - 96.1%) respectively. An almost perfect agreement was found between both modalities regarding the diagnosis of morphology (Kappa: 0.84) and severity (Kappa: 0.86) of perfusion defects. On DECT images, there was almost perfect agreement between both readers for morphology (Kappa: 0.94) and severity (Kappa: 0.89). In addition, a significantly sharper delineation of the perfusion defects on DECT images (mean score: 3.9; range: 3-4) was found in comparison to SPECT images (mean: 2.9; range: 2-3) ($P < 0.0001$). These results are illustrated in **Figure 6 and 7**.

Radiation dose

The mean estimated equivalent dose was 4.1 ± 2.3 (SD) mSv (range: 1.9-11.85 mSv) for DECT and 5.3 ± 1.1 (SD) mSv (range: 2.8-7.3 mSv) for SPECT-CT. This corresponded to a significant equivalent dose reduction of 21.2% ($P = 0.0004$) for DECT compared to SPECT-CT.

Discussion

The present study found a strong correlation between quantitative DECT lung perfusion and SPECT-CT with high accuracy and also almost perfect agreement in detection of lung perfusion defects. Nevertheless, our results should be interpreted in a wider context of contradictory literature comparing various scintigraphy methods to DECT for qualitative lung perfusion imaging. For instance, while we found very good sensitivity (89.4%) for depiction of pulmonary perfusion defects, a previous study on 15 patients reported that the sensitivity for iodine maps was 76.7% in comparison to SPECT-CT(11). This difference may be explained by the use of recent technological developments that provide a full field-of-view, thus overcoming the spatial limitation of older DECT systems.

In addition, we found almost perfect agreements in the number, morphology, and severity of pulmonary perfusion defects between DECT and SPECT-CT. These findings contrast previous with studies(10,14,15,18), in particular with one study that, despite the use of a 3D SPECT-CT modality, demonstrated a fair inter-modality concordance at a segmental level

(Kappa: 0.25) on 19 patients with known CTEPH (18). This finding may be explained, at least in part, by the rate of non-diagnostic lung segments (5.5%) due to streak artifacts which was much greater than in our study, probably owing to the higher iodinated contrast volume used as evidenced by persistence of contrast in the superior vena cava. Furthermore, the inter-modality agreement reported in our study was based on the findings of a nuclear physician, which possibly avoided interpretation bias and ensured that the modality of comparison was the current gold standard. We also found excellent concordance for iodine map interpretation between the nuclear physician and the diagnostic radiologist indicating the feasibility of a non-expert reader evaluation of perfusion abnormalities.

Our study has demonstrated for the first time a strong correlation of the relative lobar perfusion measured via the concentration of iodine in DECT and the quantity of radiotracer in SPECT-CT. It is of note to mention that a recent study compared the quantification of perfusion on DECT and SPECT-CT but in terms of HU (18). In this study, the authors found poor correlation (*r* ranged from 0.01 to 0.45) among the lobes studied (18) whereas, in our study, excellent correlation was found. This may be explained by the DECT modality that allows accurate quantification of the iodinated contrast media and easily differentiates it from underlying lung tissue, contrary to the conventional HU images (24). In our study there were, however, certain differences in the results between lobes; a lower accuracy in the middle lobe, and larger limits of agreement in the basal lobes were observed. Both findings could be explained by spatial misregistration between SPECT and CT scans due to longer acquisition times with free-breathing (19). This highlights a strong advantage of DECT which allows a perfect registration of the perfusion blood volume into a 3D volume because of the native simultaneous iodine and conventional HU image registration.

The differences found in the present study between DECT and SPECT-CT may be related to several technical aspects. For instance, the contrast agent used in DECT has fast passive diffusion because of its small molecular weight, while with scintigraphy the radiotracer will be retained in the pulmonary parenchyma capillaries because of their large size (32). Therefore, for DECT the iodine concentration within a volume reflects the perfusion blood volume, which is not *stricto sensu* perfusion imaging, but rather a marker of functional capillary density, described as micro angiography imaging (32). On the opposite, with SPECT the radiotracer is a good marker of perfusion, making it the standard of reference. The difference in contrast agent distribution has been reported to be particularly marked in the presence of a systemic collateral blood supply that is encountered in CTEPH

(33). Another point to consider is that the comparison between the imaging modalities could be hampered by the quantitative accuracy known to be not flawless; for DECT, a bias less than 5% for a concentration up to 1 mg/mL has been reported at radiation dose similar to that used in the present study(24–26), and for CZT-based pre-clinical SPECT, errors of up to approximately 5.45% with an energy window of 10% in the estimation of the radioactivity concentration for a range of radionuclides has been reported (34). In addition, the difference in spatial resolution could also explain qualitative disagreements in diagnosis of perfusion defects due to partial volume effects expected with SPECT-CT, even with new CZT camera technology(35,36).

In our study, SPECT-CT imaging exposed patients to a significantly higher radiation dose than DECT, as reported in another study in which the mean equivalent doses for DECT and SPECT-CT were 5.1 ± 1.3 (SD) mSv and 8.2 ± 2.1 (SD) mSv, respectively (18). This is likely explained by the combination of two scans for SPECT-CT. On the other hand, DECT allows a radiation dose corresponding to a conventional CT due to dual layer technology (26).

Our study has several limitations. For example, lobe segmentations could have suffered from mis-delineation of the fissures, as discussed above. However, this was minimized by evaluating the lobar segmentation in consensus. Another limitation is that the number of segments with a perfusion defect was lower than those without. Nevertheless, nearly two-thirds of the patients presented with a perfusion defect; in addition, more than a thousand segments were analyzed without any exclusions from statistical analysis. Another point to note is that we did not investigate the ventilation SPECT imaging, but this was beyond the scope of the study. Finally, the diagnostic value of the quantitative and qualitative pulmonary DECT perfusion imaging for pulmonary vascular diseases such as chronic thromboembolic pulmonary hypertension and pulmonary hypertension would have to be addressed in further studies, with or without the combination of lung Xenon ventilation DECT acquisitions.

In conclusion, the head-to-head comparison of lung perfusion imaging derived from DECT and SPECT-CT modalities demonstrated strong agreements in qualitative analysis and strong correlations for quantitative analysis. One of the main advantages in clinical use is that DECT lung perfusion imaging can be added to the workflow as a substitute or complementary examination to scintigraphy for various thoracic applications such as pulmonary hypertension or prediction of post-operative lung function.

Aknowledgements

We thank Dr. Riham Dessouky, Dr. Benjamin Matagrin, Philip Robinson and Thomas Broussaud for proof reading the article.

Conflicts of interest

The authors declare that they have no conflicts of interest to disclose in relation with this article.

REFERENCES

1. Bajc M, Neilly JB, Miniati M, Schuemichen C, Meignan M, Jonson B. EANM guidelines for ventilation/perfusion scintigraphy : Part 2. Algorithms and clinical considerations for diagnosis of pulmonary emboli with V/P(SPECT) and MDCT. Eur J Nucl Med Mol Imaging 2009;36:1528–38.

2. Mineo TC, Schillaci O, Pompeo E, Mineo D, Simonetti G. Usefulness of lung perfusion scintigraphy before lung cancer resection in patients with ventilatory obstruction. Ann Thorac Surg 2006;82:1828–34.

3. Kovacević-Kuśmierek K, Kozak J, Pryt Ł, Bieńkiewicz M, Cichocki P, Kuśmierek J, et al. Perfusion lung scintigraphy for the prediction of postoperative residual pulmonary function in patients with lung cancer. Nucl Med Rev Cent East Eur 2015;18:70–7.

4. Hayashino Y, Goto M, Noguchi Y, Fukui T. Ventilation-perfusion scanning and helical CT in suspected pulmonary embolism: meta-analysis of diagnostic performance. Radiology 2005;234:740–8.

5. Verschakelen JA, Bogaert J, De Wever W. Computed tomography in staging for lung cancer. Eur Respir J Suppl 2002;35:40s–8s.

6. Ludes C, Labani A, Severac F, Jeung MY, Leyendecker P, Roy C, et al. Ultra-low-dose unenhanced chest CT: prospective comparison of high kV/low mA versus low kV/high mA protocols. Diagn Interv Imaging 2019;100:85–93.

7. Fillon M, Si-Mohamed S, Coulon P, Vuillod A, Klahr P, Boussel L. Reduction of patient radiation dose with a new organ based dose modulation technique for thoraco-abdominopelvic computed tomography (CT) (Liver dose right index). Diagn Interv Imaging 2018;99:483–92.

8. Si-Mohamed SA, Douek PC, Boussel L. Spectral CT: Dual energy CT towards multienergy CT. J Imag Diagn Interv 2019;2:32–45.

9. Fuld MK, Halaweish AF, Haynes SE, Divekar AA, Guo J, Hoffman EA. Pulmonary perfused blood volume with dual-energy CT as surrogate for pulmonary perfusion assessed with dynamic multidetector CT. Radiology 2013;267:747–56.

10. Tang CX, Yang GF, Schoepf UJ, Han ZH, Qi L, Zhao YE, et al. Chronic thromboembolic pulmonary hypertension: comparison of dual-energy computed tomography and single photon emission computed tomography in canines. Eur J Radiol 2016;85:498–506.

11. Thieme SF, Becker CR, Hacker M, Nikolaou K, Reiser MF, Johnson TRC. Dual energy CT for the assessment of lung perfusion--correlation to scintigraphy. Eur J Radiol 2008;68:369–74.

12. Giordano J, Khung S, Duhamel A, Hossein-Foucher C, Bellèvre D, Lamblin N, et al. Lung perfusion characteristics in pulmonary arterial hypertension (PAH) and peripheral forms of chronic thromboembolic pulmonary hypertension (pCTEPH): dual-energy CT experience in 31 patients. Eur Radiol 2017;27:1631–9.

13. Nakazawa T, Watanabe Y, Hori Y, Kiso K, Higashi M, Itoh T, et al. Lung perfused blood volume images with dual-energy computed tomography for chronic thromboembolic pulmonary hypertension: correlation to scintigraphy with single-photon emission computed tomography. J Comput Assist Tomogr. 2011;35:590–5.

14. Dournes G, Verdier D, Montaudon M, Bullier E, Rivière A, Dromer C, et al. Dual-energy CT perfusion and angiography in chronic thromboembolic pulmonary hypertension: diagnostic accuracy and concordance with radionuclide scintigraphy. Eur Radiol. 2014;24:42–51.

15. Masy M, Giordano J, Petyt G, Hossein-Foucher C, Duhamel A, Kyheng M, et al. Dual-energy CT (DECT) lung perfusion in pulmonary hypertension: concordance rate with V/Q scintigraphy in diagnosing chronic thromboembolic pulmonary hypertension (CTEPH). Eur Radiol 2018;28:5100–10.

16. Thieme SF, Graute V, Nikolaou K, Maxien D, Reiser MF, Hacker M, et al. Dual-energy CT lung perfusion imaging--correlation with SPECT/CT. Eur J Radiol 2012;81:360–5.

17. Koike H, Sueyoshi E, Sakamoto I, Uetani M, Nakata T, Maemura K. Comparative clinical and predictive value of lung perfusion blood volume CT, lung perfusion SPECT and catheter pulmonary angiography images in patients with chronic thromboembolic pulmonary hypertension before and after balloon pulmonary angioplasty. Eur Radiol 2018;28:5091–9.

18. Renapurkar RD, Bolen MA, Shrikanthan S, Bullen J, Karim W, Primak A, et al. Comparative assessment of qualitative and quantitative perfusion with dual-energy CT and planar and SPECT-CT

V/Q scanning in patients with chronic thromboembolic pulmonary hypertension. Cardiovasc Diagn Ther 2018;8:414–22.

19. Roach PJ, Schembri GP, Bailey DL. V/Q scanning using SPECT and SPECT/CT. J Nucl Med Off Publ Soc Nucl Med 2013;54:1588–96.

20. Provost K, Leblond A, Gauthier-Lemire A, Filion É, Bahig H, Lord M. Reproducibility of lobar perfusion and ventilation quantification using SPECT/CT segmentation software in lung cancer patients. J Nucl Med Technol 2017;45:185–92.

21. Toney LK, Wanner M, Miyaoka RS, Alessio AM, Wood DE, Vesselle H. Improved prediction of lobar perfusion contribution using technetium-99m-labeled macroaggregate of albumin single photon emission computed tomography/computed tomography with attenuation correction. J Thorac Cardiovasc Surg 2014;148:2345–52.

22. Park SJ, Yu AR, Kim YS, Kang WS, Jin SS, Kim JS, et al. Evaluation of quantitative accuracy in CZT-based pre-clinical SPECT for various isotopes. J Instrum 2015;10:T05004–T05004.

23. Goshen E, Beilin L, Stern E, Kenig T, Goldkorn R, Ben-Haim S. Feasibility study of a novel general purpose CZT-based digital SPECT camera: initial clinical results. EJNMMI Phys 2018;5:6.

24. Hua CH, Shapira N, Merchant TE, Klahr P, Yagil Y. Accuracy of electron density, effective atomic number, and iodine concentration determination with a dual-layer dual-energy computed tomography system. Med Phys 2018;45:2486–97.

25. Kim H, Goo JM, Kang CK, Chae KJ, Park CM. Comparison of iodine density measurement among dual-energy omputed tomography scanners from 3 vendors. Invest Radiol 2018;53:321–7.

26. Ehn S, Sellerer T, Muenzel D, Fingerle AA, Kopp F, Duda M, et al. Assessment of quantification accuracy and image quality of a full-body dual-layer spectral CT system. J Appl Clin Med Phys 2018;19:204–17.

27. Colevray M, Tatard-Leitman VM, Gouttard S, Douek P, Boussel L. Convolutional neural network evaluation of over-scanning in lung computed tomography. Diagn Interv Imaging 2019;100:177–83.

28. Boyden EA. Segmental anatomy of the lungs: a study of the patterns of the segmental bronchi and related pulmonary vessels. New York: McGraw-Hill, 1955.

29. Si-Mohamed S, Thivolet A, Bonnot P-E, Bar-Ness D, Képénékian V, Cormode DP, et al. Improved peritoneal cavity and abdominal organ imaging using a biphasic contrast agent protocol and spectral photon counting computed tomography K-edge imaging. Invest Radiol 2018;53:629–39.

30. Stamm G, Nagel HD. CT-expo: a novel program for dose evaluation in CT. ROFO 2002;174:1570–6.

31. The 2007 Recommendations of the International Commission on Radiological Protection. ICRP publication 103. Ann ICRP 2007;37:1–332.

32. Le Bihan D. Theoretical principles of perfusion imaging : application to magnetic resonance imaging. Invest Radiol 1992;27:S6-11.

33. Renard B, Remy-Jardin M, Santangelo T, Faivre J-B, Tacelli N, Remy J, et al. Dual-energy CT angiography of chronic thromboembolic disease: can it help recognize links between the severity of pulmonary arterial obstruction and perfusion defects? Eur J Radiol 2011;79:467–72.

34. Willowson K, Bailey DL, Baldock C. Quantitative SPECT reconstruction using CT-derived corrections. Phys Med Biol 2008;53:3099–112.

35. Liu X, Persson M, Bornefalk H, Karlsson S, Xu C, Danielsson M, et al. Spectral response model for a multibin photon-counting spectral computed tomography detector and its applications. J Med Imaging 2015;2:033502.

36. Gregoire B, Pina-Jomir G, Bani-Sadr A, Moreau-Triby C, Janier M, Scheiber C. Four-minute bone SPECT using large-field cadmium-zinc-telluride camera. Clin Nucl Med 2018;43:389–95.

FIGURE and tables CAPTIONS

Figure 1. Flow chart shows inclusion/exclusion process.

Figure 2. Lobar segmentation using Q.Lung® (GE Healthcare) for scintigraphy photon emission computed tomography-computed tomography (SPECT-CT) images (upper row, A: axial, B: coronal, C: sagittal) and COPD software (IntelliSpace Portal; Philips Healthcare) for dual-layer dual energy computed tomography (DECT) images (lower row, D: axial, E: coronal, F: sagittal). A specific color has been attributed for each mask for easy recognition of the lobes.

Figure 3. Graphs show linear regression (A) and Bland-Altman analysis (B) between the relative lobar perfusion measured with dual-layer dual energy computed tomography (DECT) and scintigraphy photon emission computed tomography-computed tomography (SPECT-CT) for the overall lobes.

Figure 4. Graphs show linear regression between the relative lobar perfusion measured with dual-layer dual energy computed tomography (DECT) and scintigraphy photon emission computed tomography-computed tomography (SPECT-CT) for each lobe.

Figure 5. Graphs show Bland-Altman analysis between the relative lobar perfusion measured with dual-layer dual energy computed tomography (DECT) and scintigraphy photon emission computed tomography-computed tomography (SPECT-CT) for each lobe.

Figure 6. Axial and coronal scintigraphy photon emission computed tomography-computed tomography (SPECT-CT) images (first and third columns) and dual-layer dual energy computed tomography (DECT) images (second and fourth columns) overlay images of a 74-year-old woman with pulmonary hypertension who had no perfusion abnormality (upper row: upper lobes, middle row: middle lobes, lower row: lower lobes). Normoperfused areas are perfectly registered on pulmonary parenchyma on DECT images, which was not the case for SPECT-CT images.

Figure 7. Axial and coronal scintigraphy photon emission computed tomography images (first and third columns) and dual-layer dual energy computed tomography images (second and fourth columns) overlay images of a 62-year-old woman with chronic thromboembolic pulmonary hypertension (upper row: upper lobes, middle row: middle lobes, lower row: lower lobes). Normoperfused and hypoperfused areas are perfectly matching between both modalities with a better depiction of the boundaries on dual-layer dual energy computed tomography images. DECT: dual-layer dual energy computed tomography SPECT-CT: scintigraphy photon emission computed tomography-computed tomography.

Table 1. Dual-layer dual energy computed tomography (DECT) and scintigraphy photon emission computed tomography-computed tomography (SPECT-CT) protocols.

Table 2. Comparison between the relative lobar perfusion measured with dual-layer dual energy computed tomography (DECT) and scintigraphy photon emission computed tomography-computed tomography (SPECT-CT).

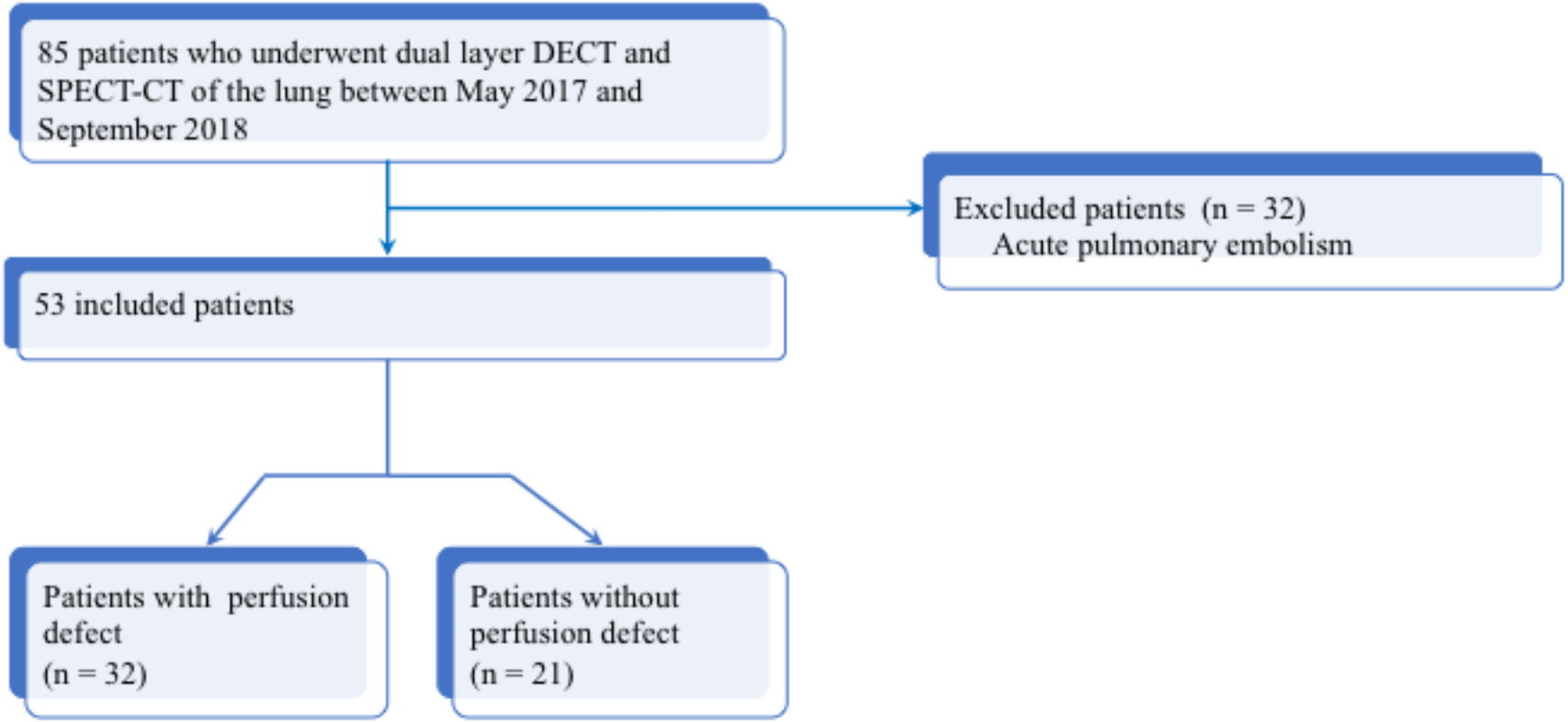
85 patients who underwent dual layer DECT and SPECT-CT of the lung between May 2017 and September 2018
Excluded patients (n = 32)
Acute pulmonary embolism
53 included patients
Patients with perfusion defect
(n = 32)
Patients without perfusion defect
(n = 21)

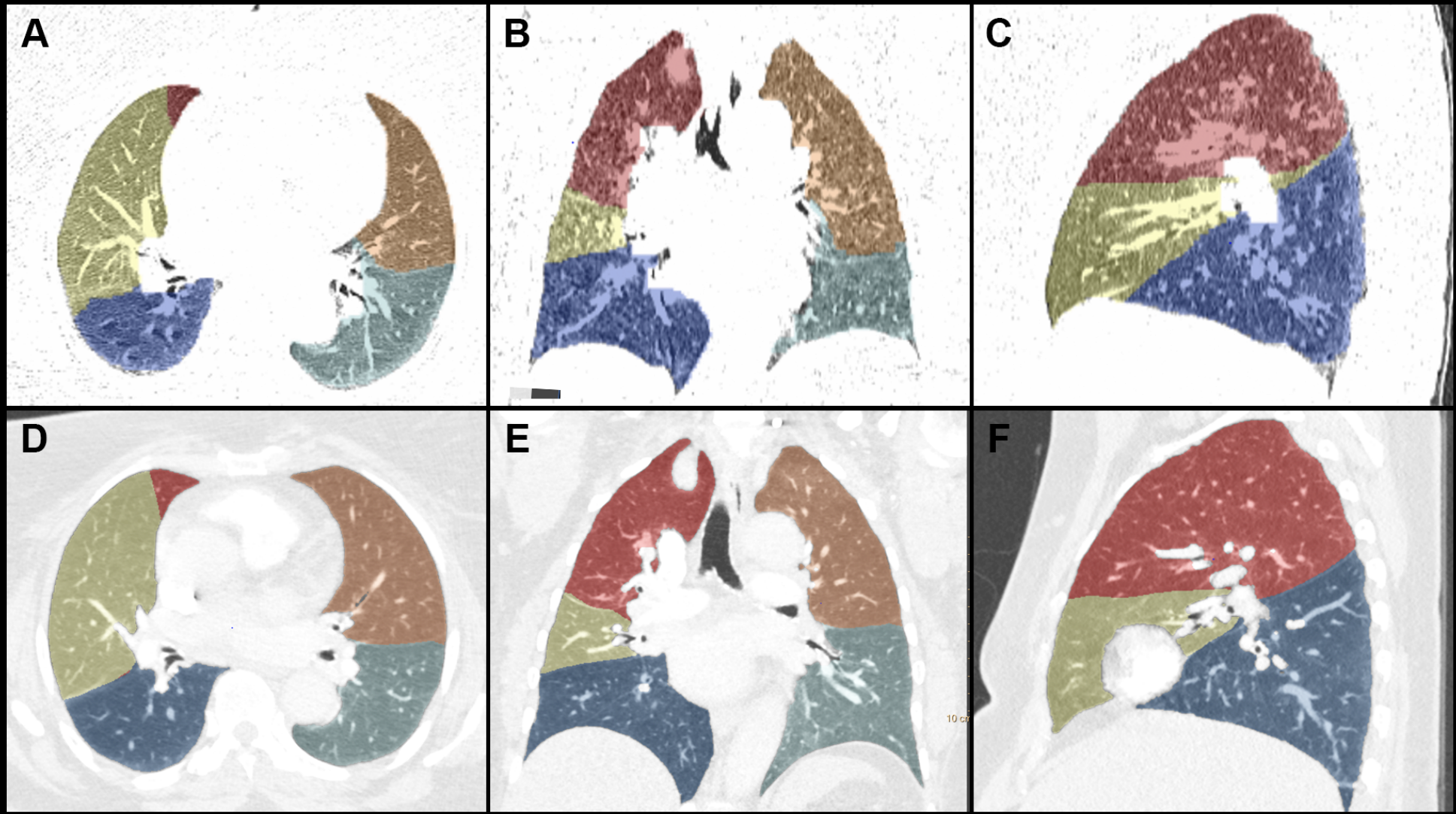
A
B
C
D
E
F

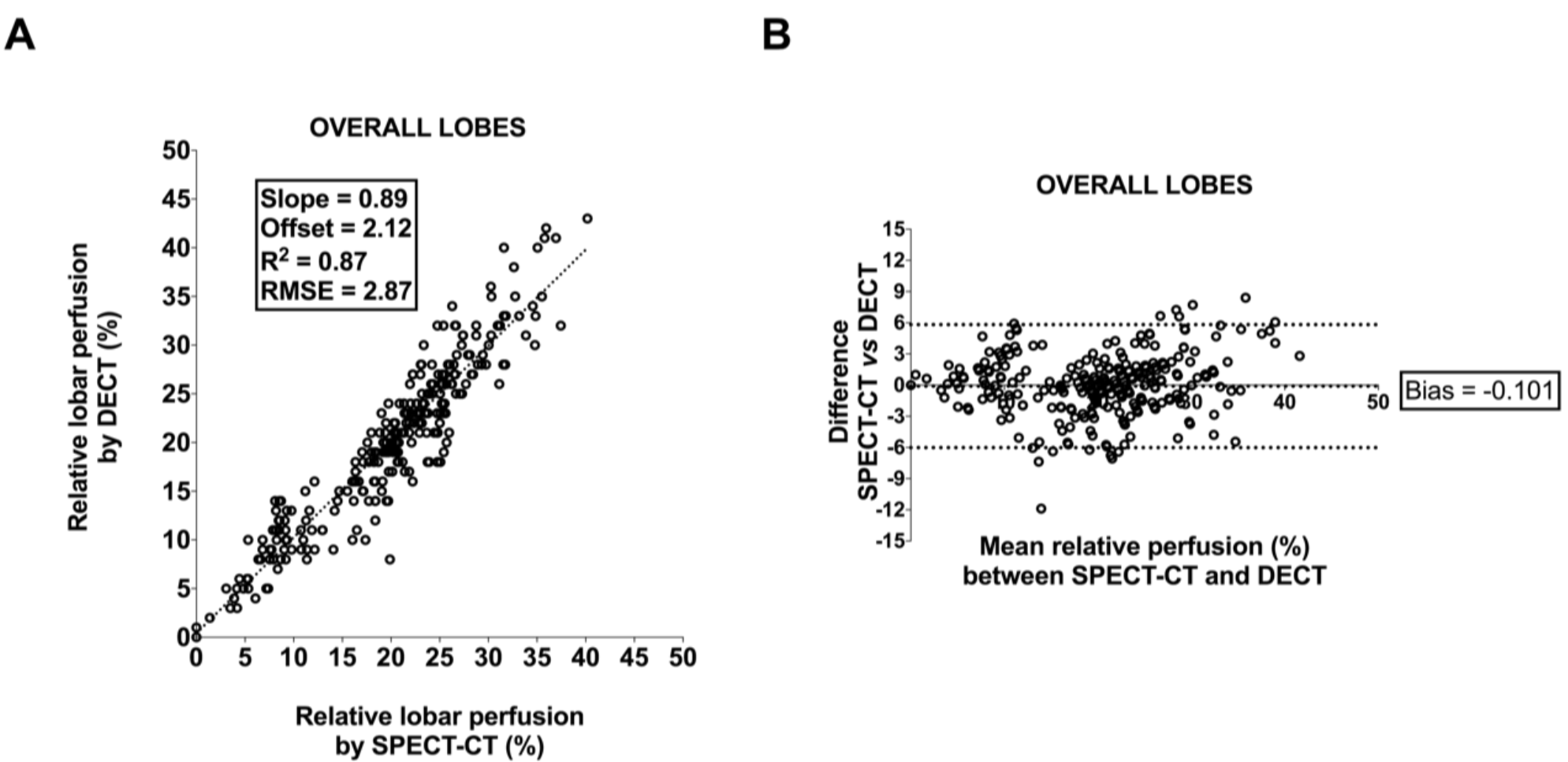
A
OVERALL LOBES
Slope = 0.89
Offset = 2.12
R2 = 0.87
RMSE = 2.87
Relative lobar perfusion by DECT (%)
Relative lobar perfusion by SPECT-CT (%)
0
5
10
15
20
25
30
35
40
45
50
B
OVERALL LOBES
Difference SPECT-CT vs DECT
Mean relative perfusion (%) between SPECT-CT and DECT
Bias = -0.101
15
12
9
6
3
0
-3
-6
-9
-12
-15
40
50

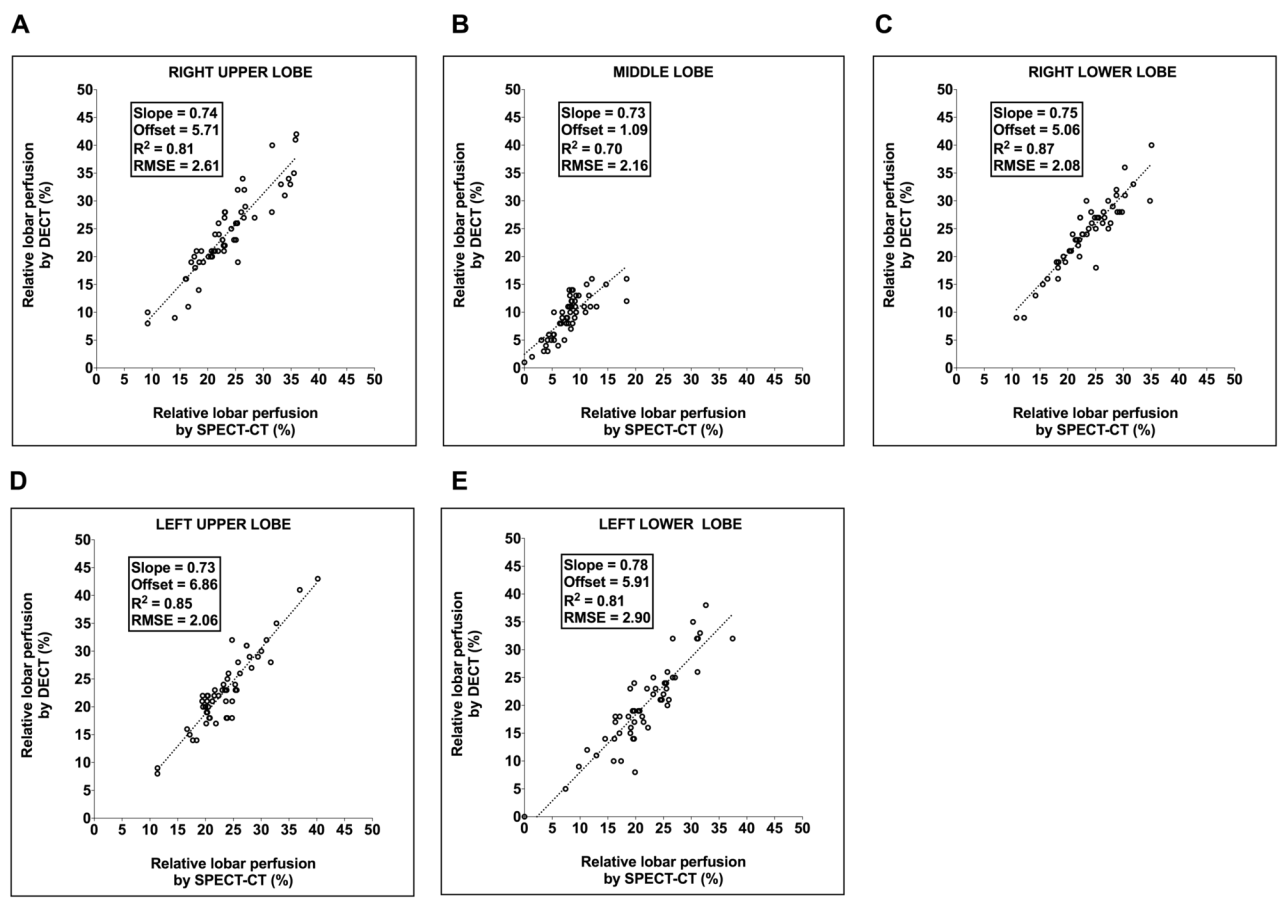
A
RIGHT UPPER LOBE
Slope = 0.74
Offset = 5.71
R2 = 0.81
RMSE = 2.61
Relative lobar perfusion by DECT (%)
Relative lobar perfusion by SPECT-CT (%)
B
MIDDLE LOBE
Slope = 0.73
Offset = 1.09
R2 = 0.70
RMSE = 2.16
Relative lobar perfusion by DECT (%)
Relative lobar perfusion by SPECT-CT (%)
C
RIGHT LOWER LOBE
Slope = 0.75
Offset = 5.06
R2 = 0.87
RMSE = 2.08
Relative lobar perfusion by DECT (%)
Relative lobar perfusion by SPECT-CT (%)
D
LEFT UPPER LOBE
Slope = 0.73
Offset = 6.86
R2 = 0.85
RMSE = 2.06
Relative lobar perfusion by DECT (%)
Relative lobar perfusion by SPECT-CT (%)
E
LEFT LOWER LOBE
Slope = 0.78
Offset = 5.91
R2 = 0.81
RMSE = 2.90
Relative lobar perfusion by DECT (%)
Relative lobar perfusion by SPECT-CT (%)

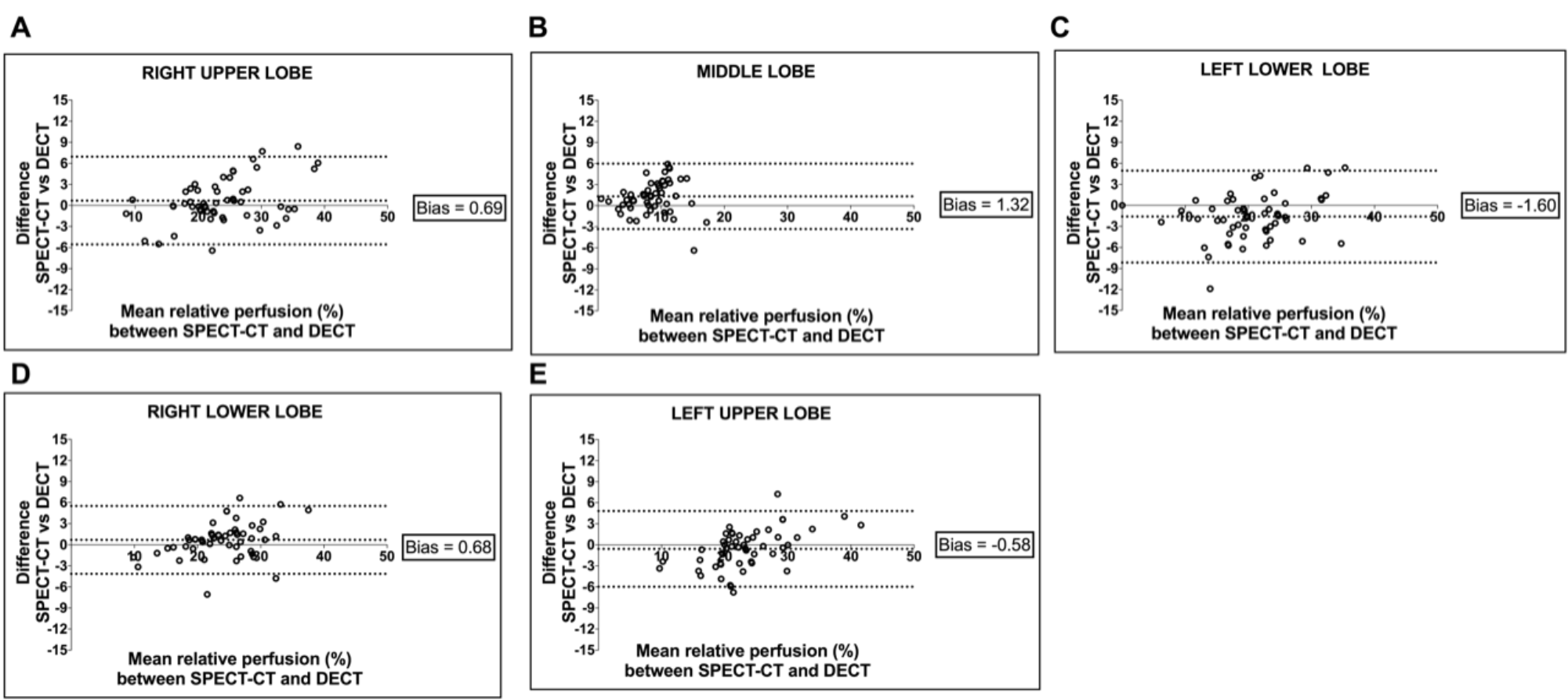
A
RIGHT UPPER LOBE
Difference SPECT-CT vs DECT
Mean relative perfusion (%) between SPECT-CT and DECT
Bias = 0.69
B
MIDDLE LOBE
Difference SPECT-CT vs DECT
Mean relative perfusion (%) between SPECT-CT and DECT
Bias = 1.32
C
LEFT LOWER LOBE
Difference SPECT-CT vs DECT
Mean relative perfusion (%) between SPECT-CT and DECT
Bias = -1.60
D
RIGHT LOWER LOBE
Difference SPECT-CT vs DECT
Mean relative perfusion (%) between SPECT-CT and DECT
Bias = 0.68
E
LEFT UPPER LOBE
Difference SPECT-CT vs DECT
Mean relative perfusion (%) between SPECT-CT and DECT
Bias = -0.58

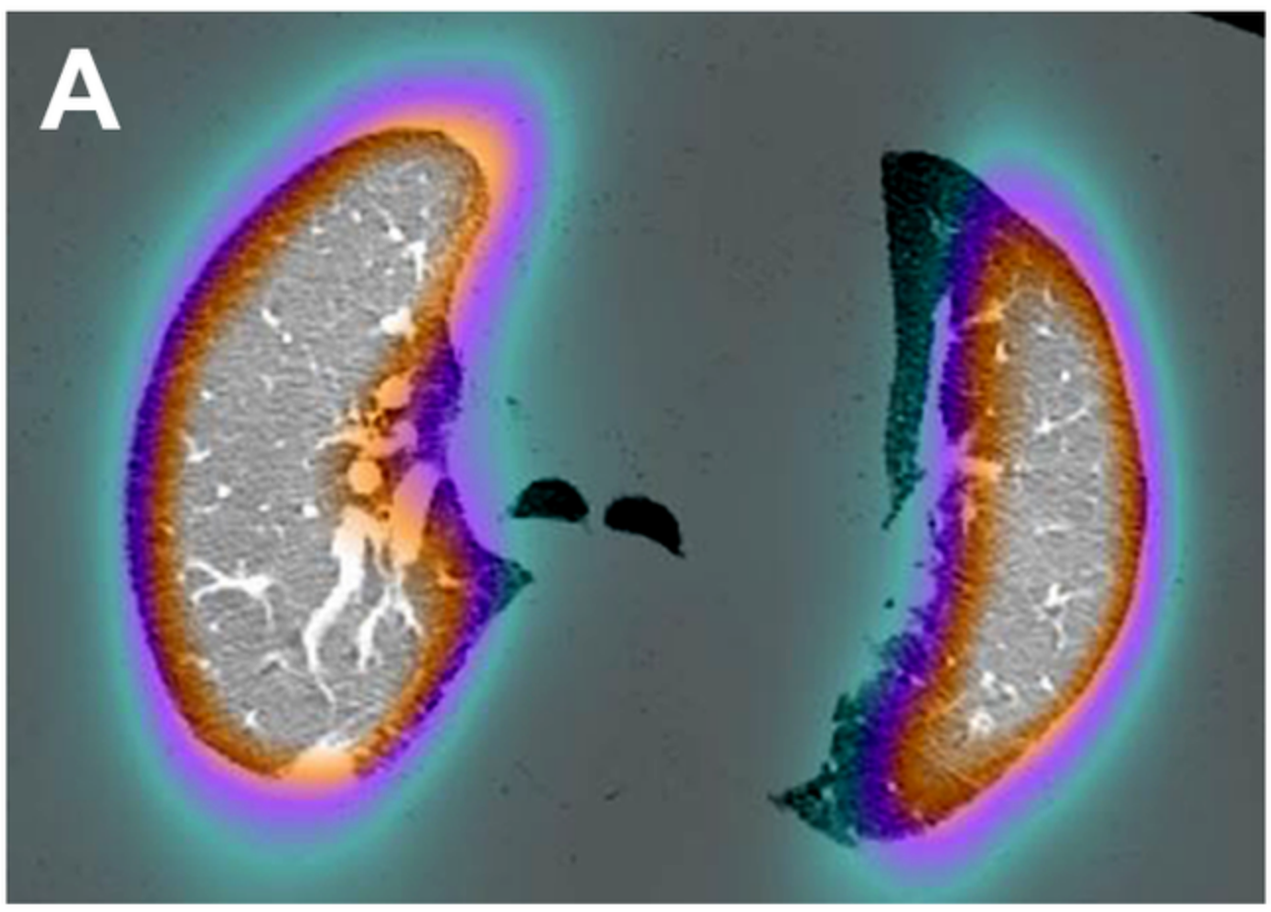
A

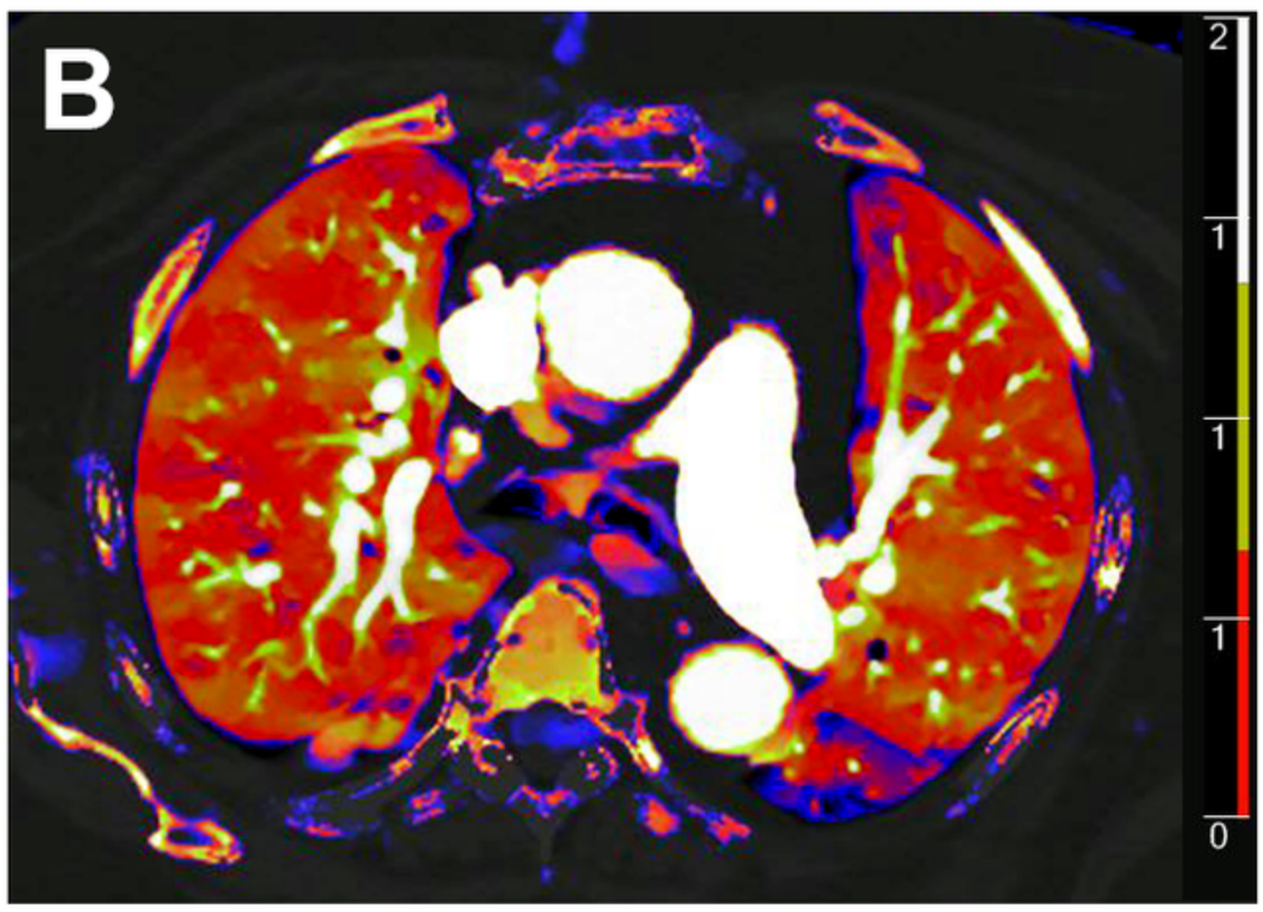
B
2
1
1
1
0

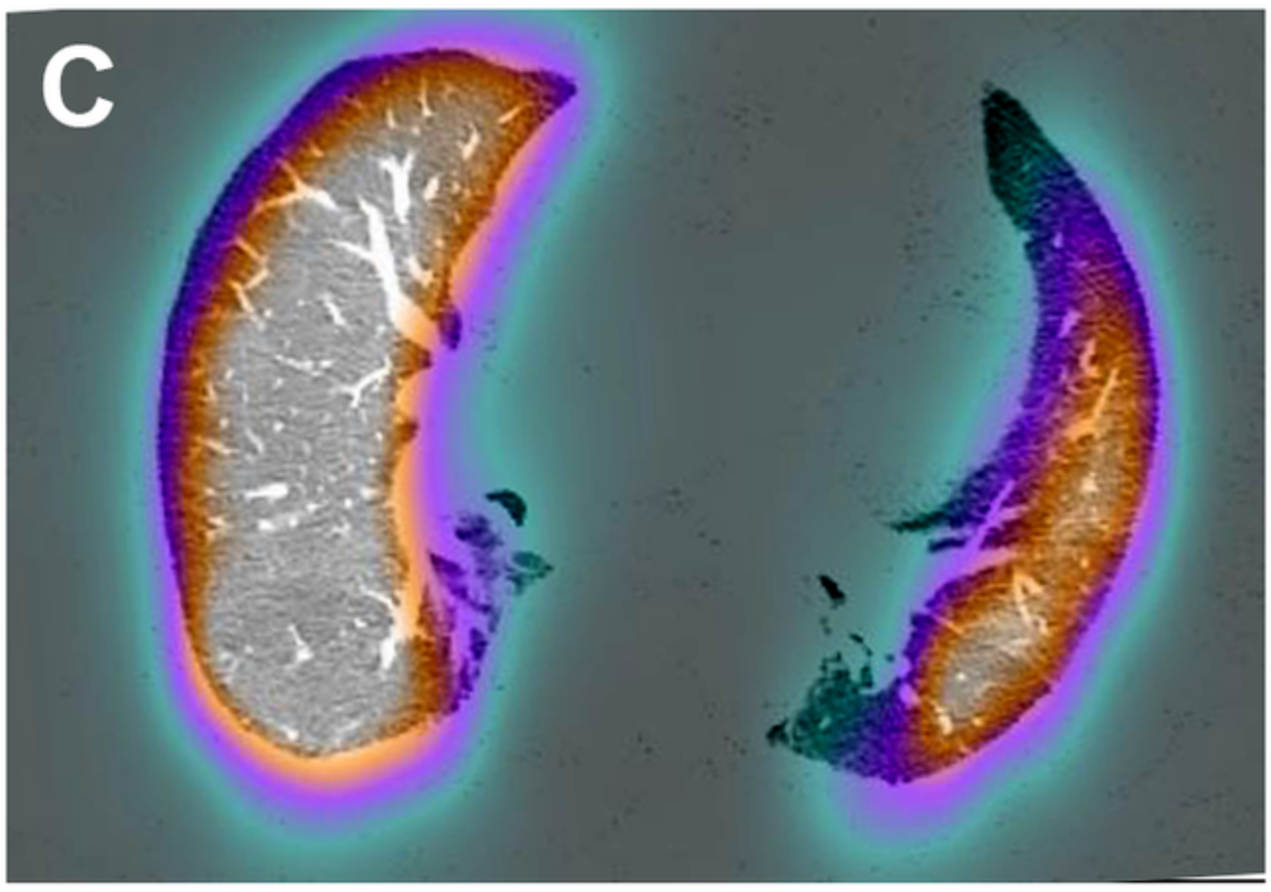
C

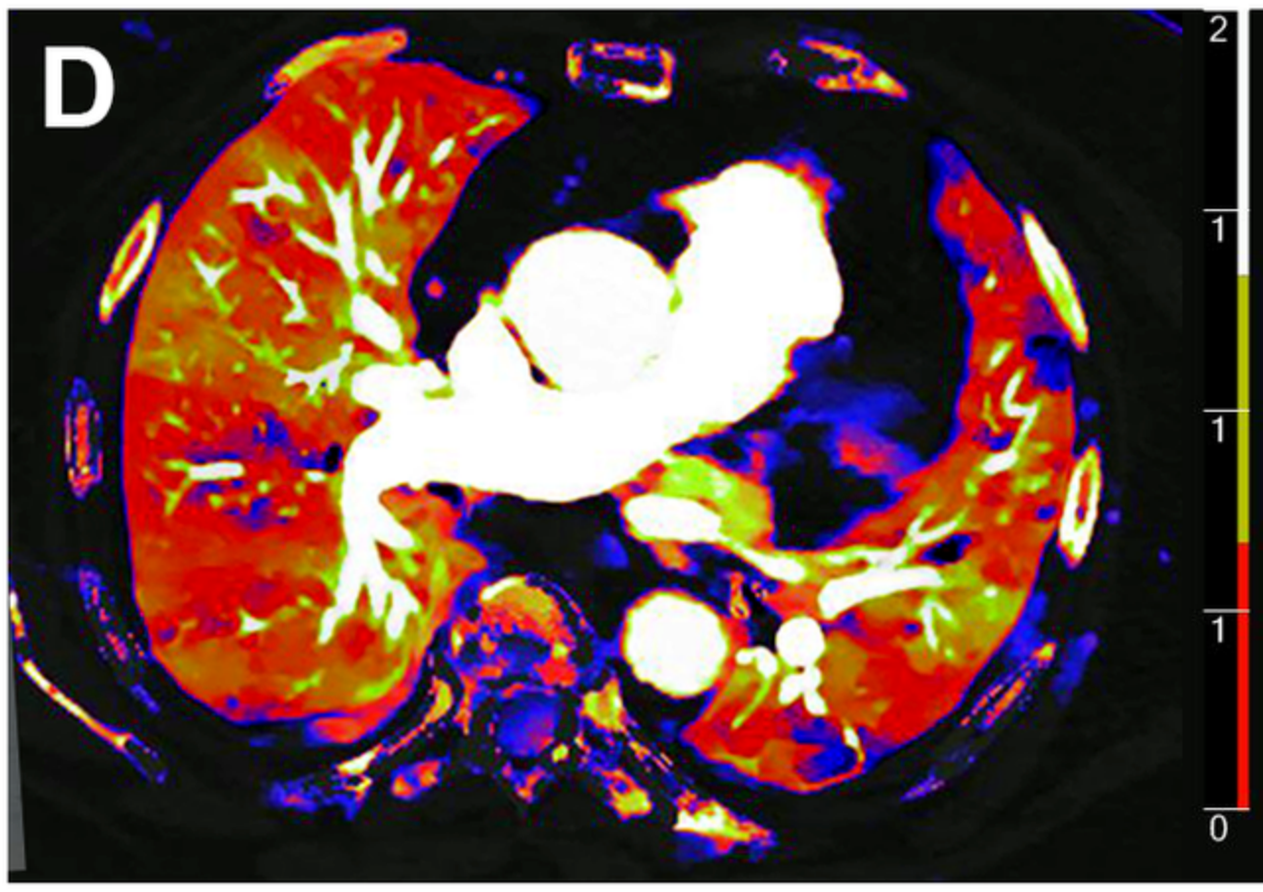
D
2
1
1
1
0

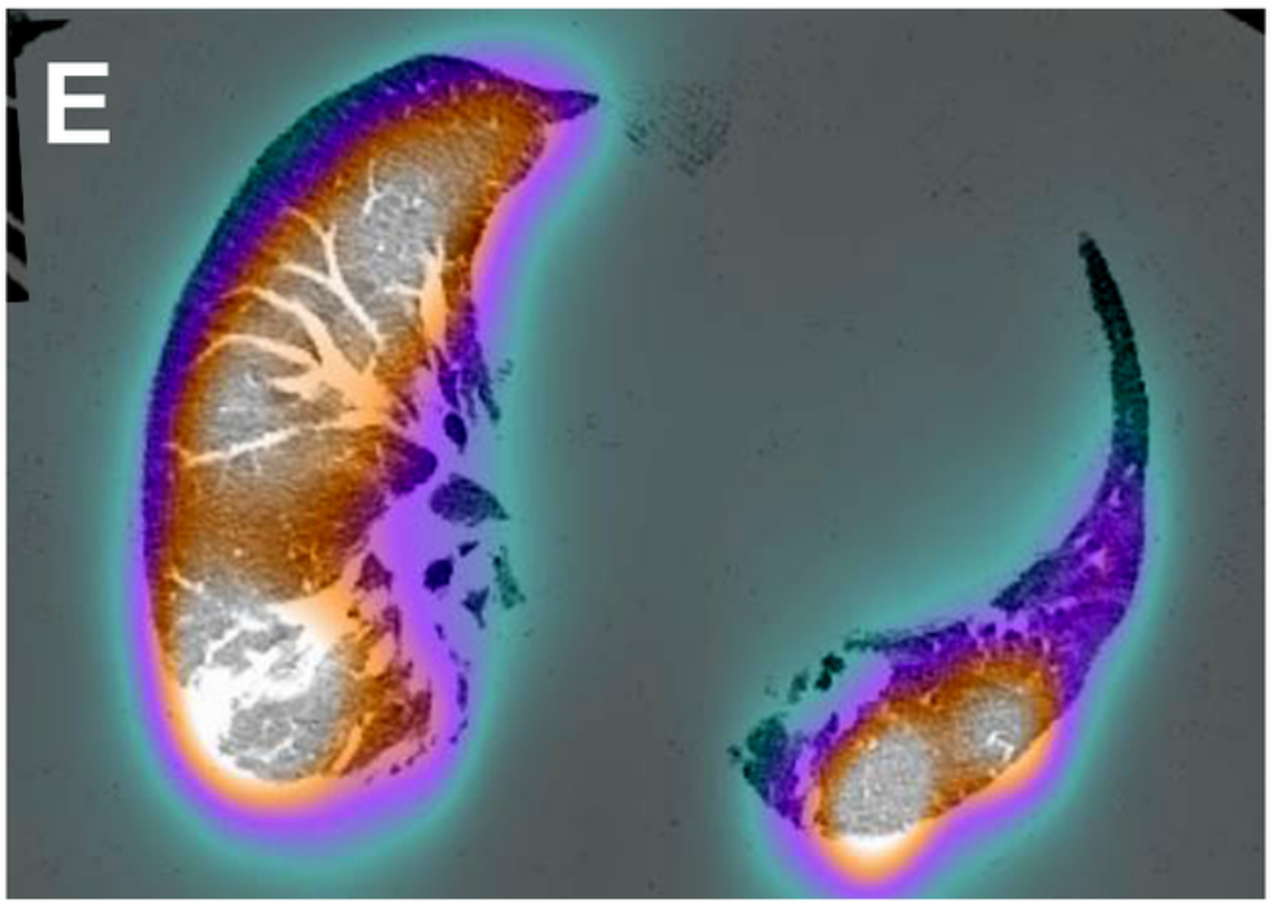
E

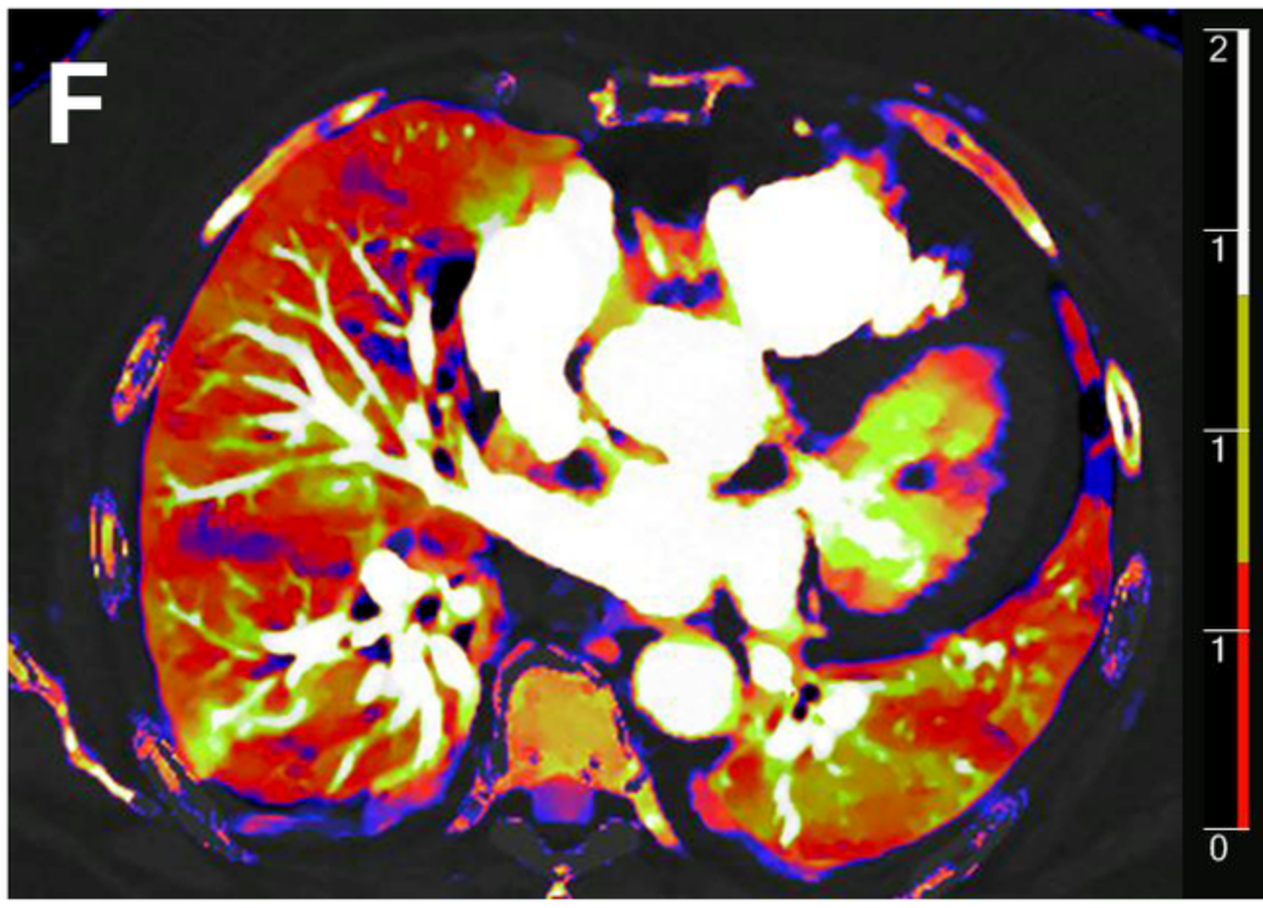
F
2
1
1
1
0

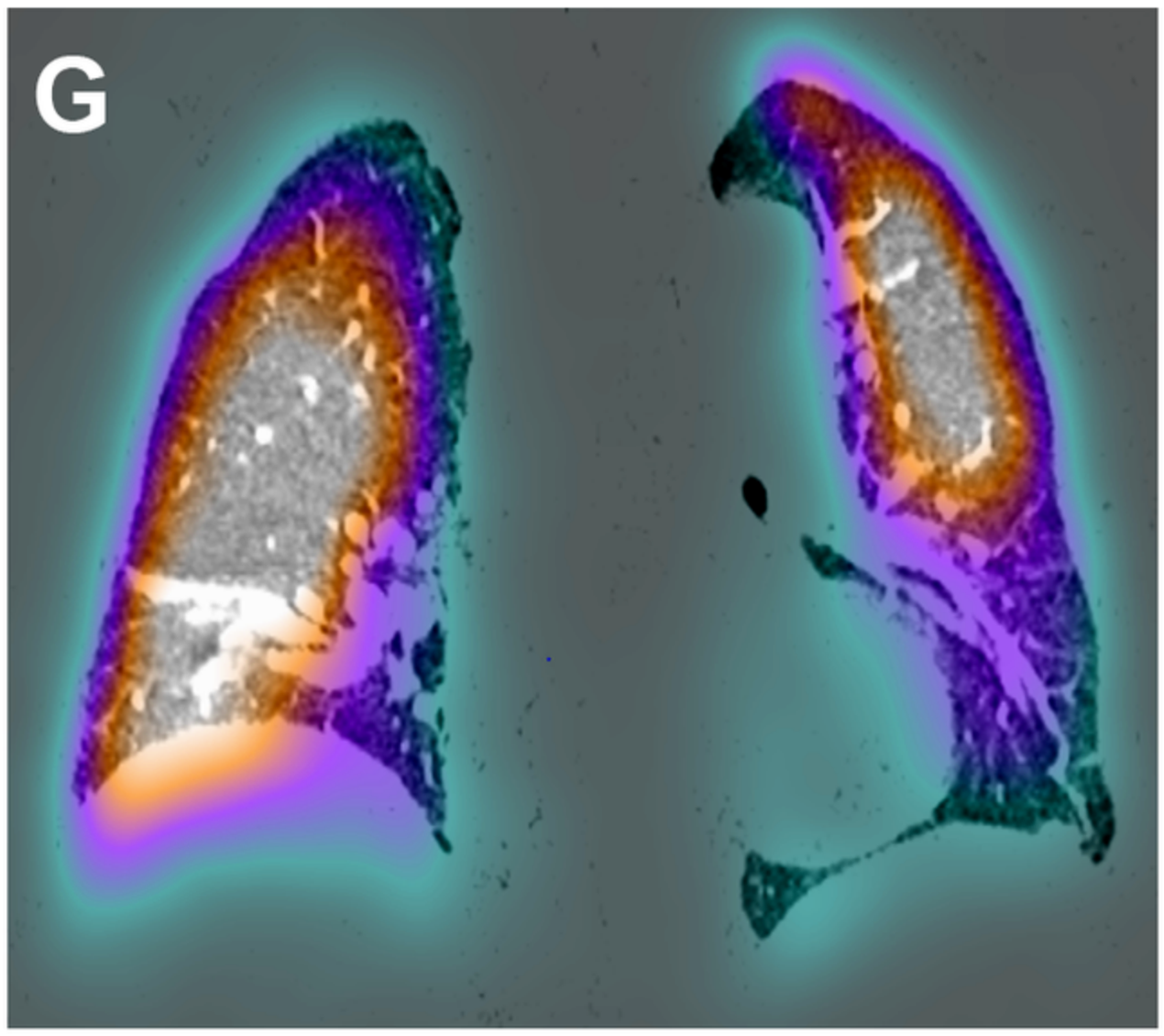
G

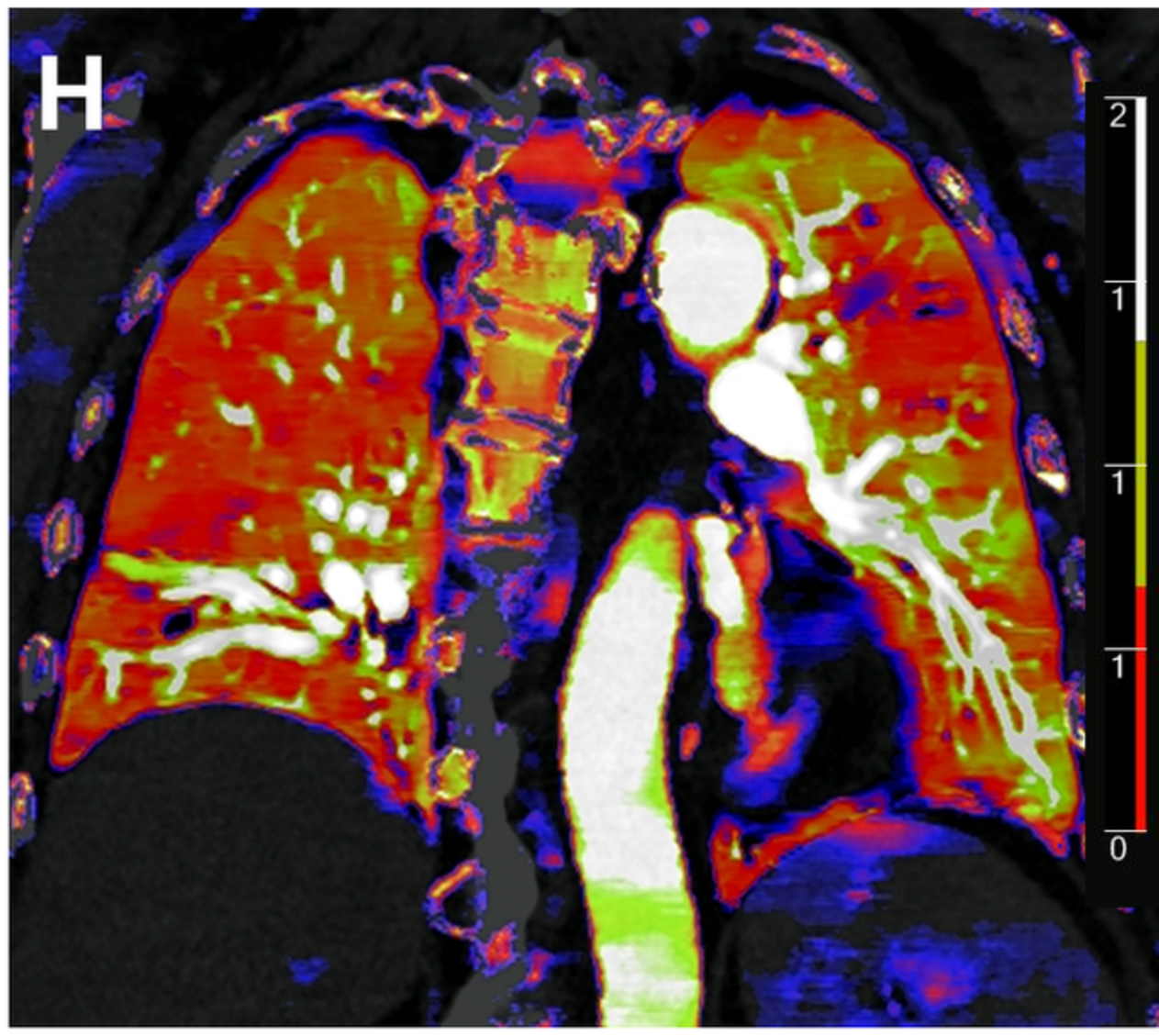
H
2
1
1
1
0

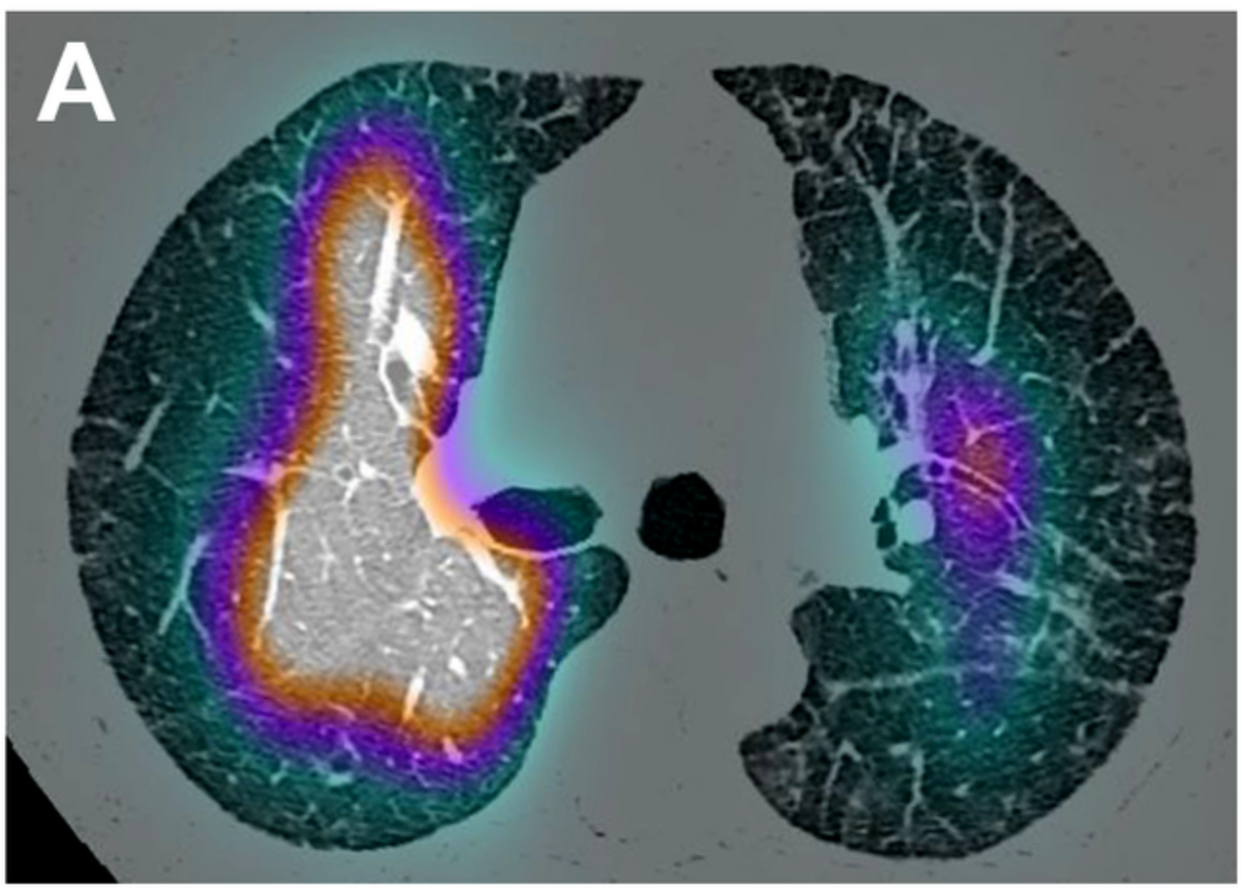
A

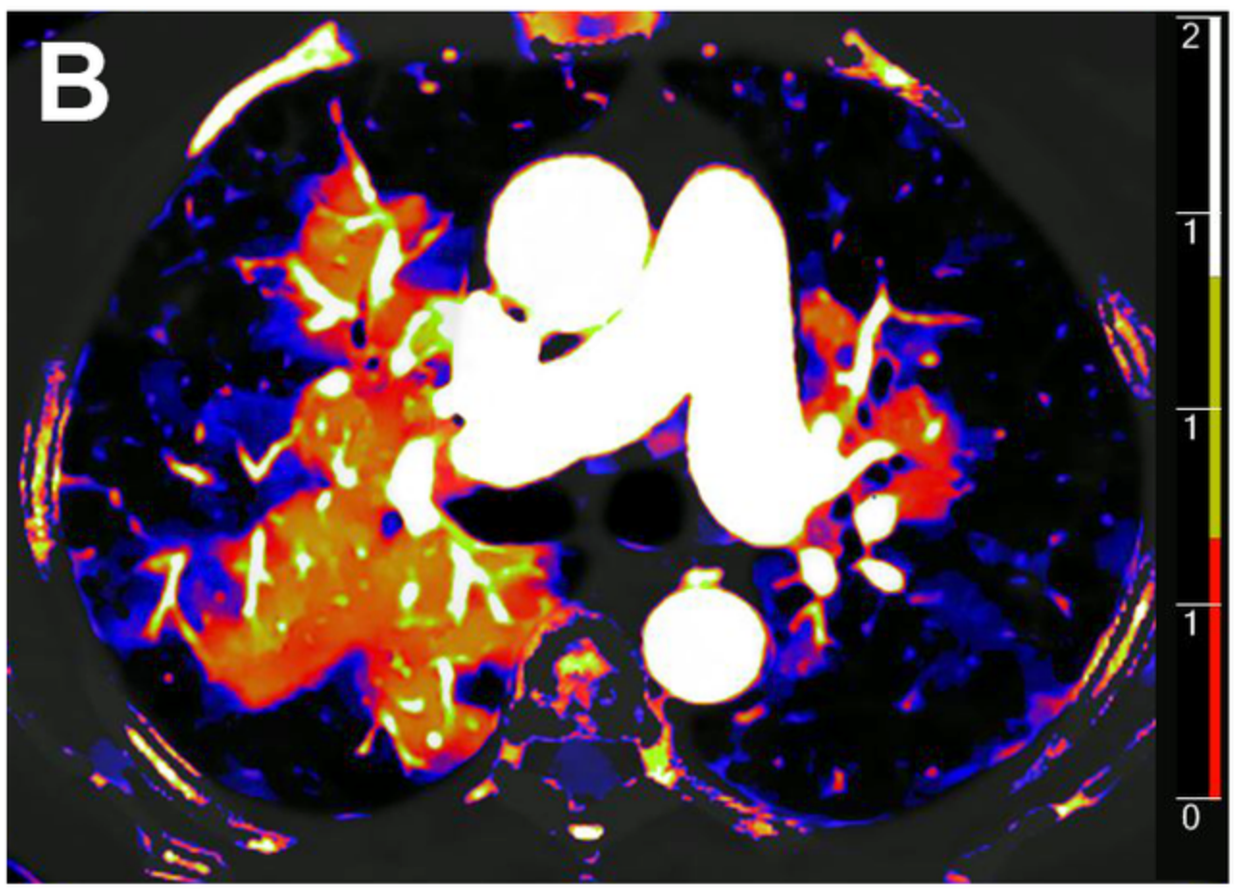
B
2
1
1
1
0

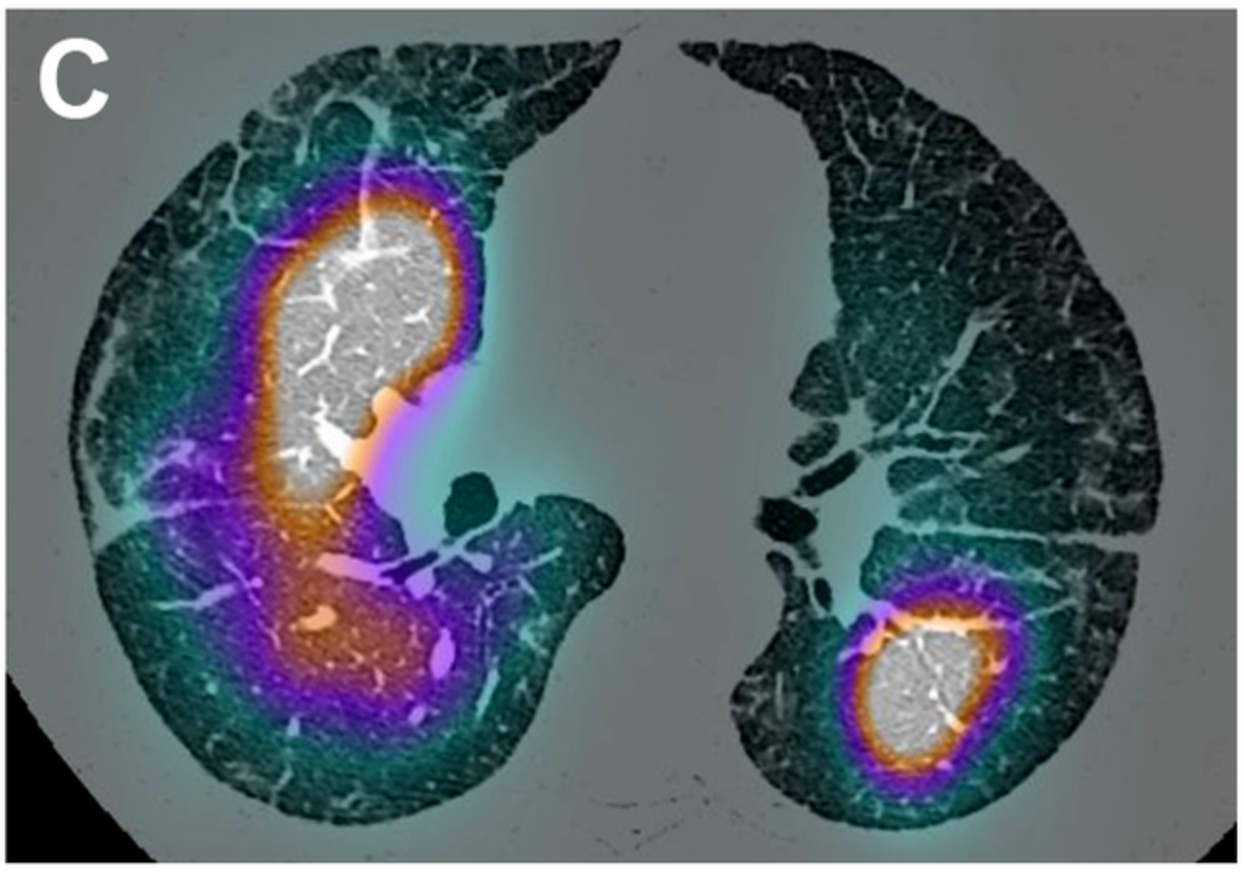
C

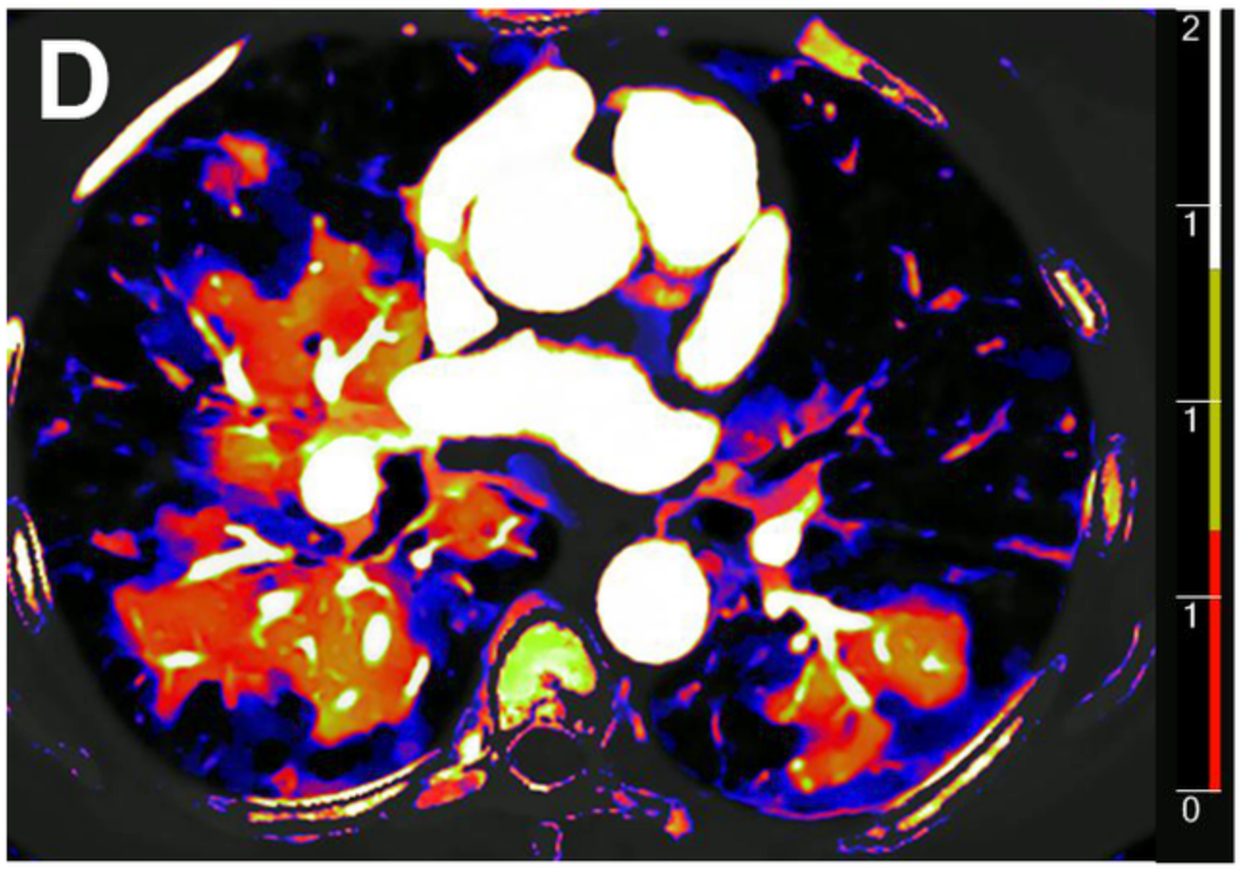
D
2
1
1
1
0

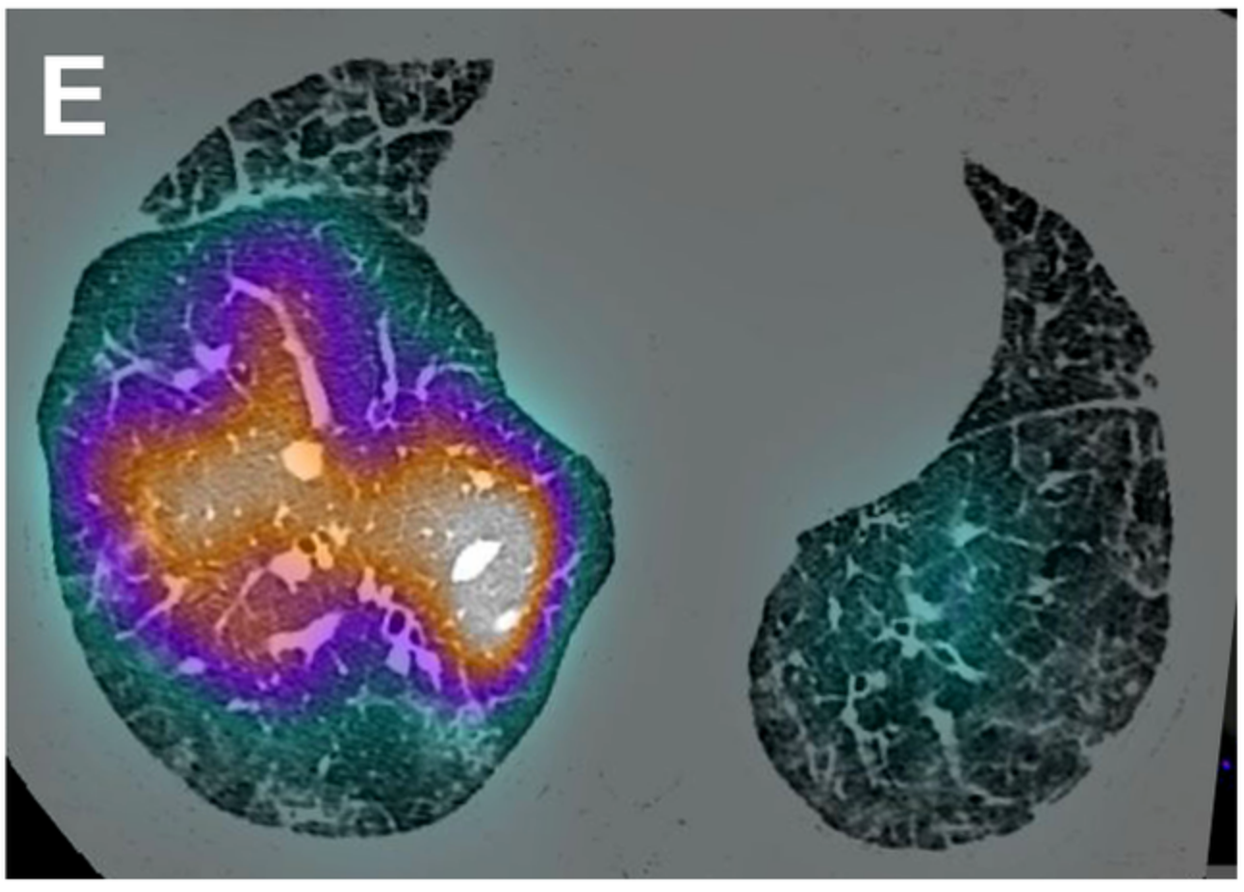
E

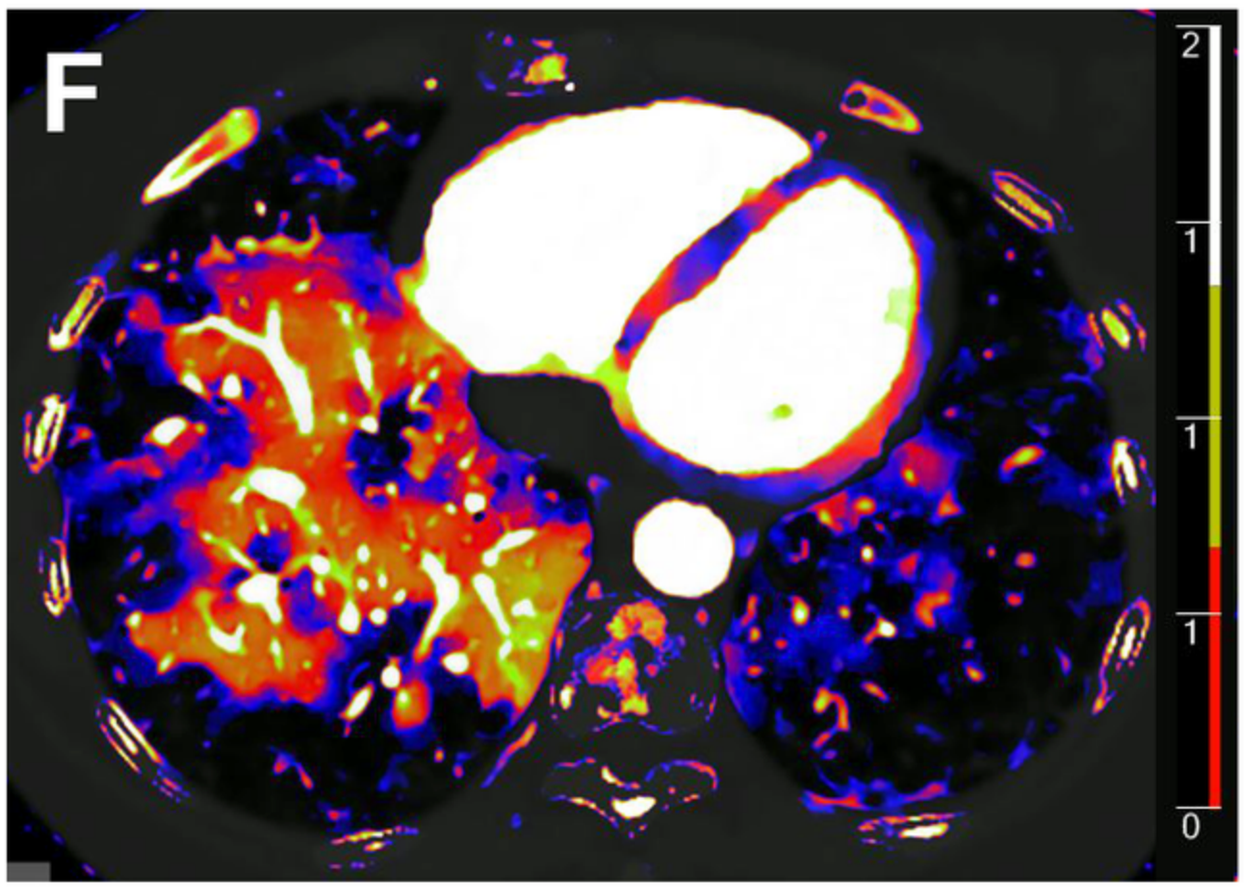
F
2
1
1
1
0

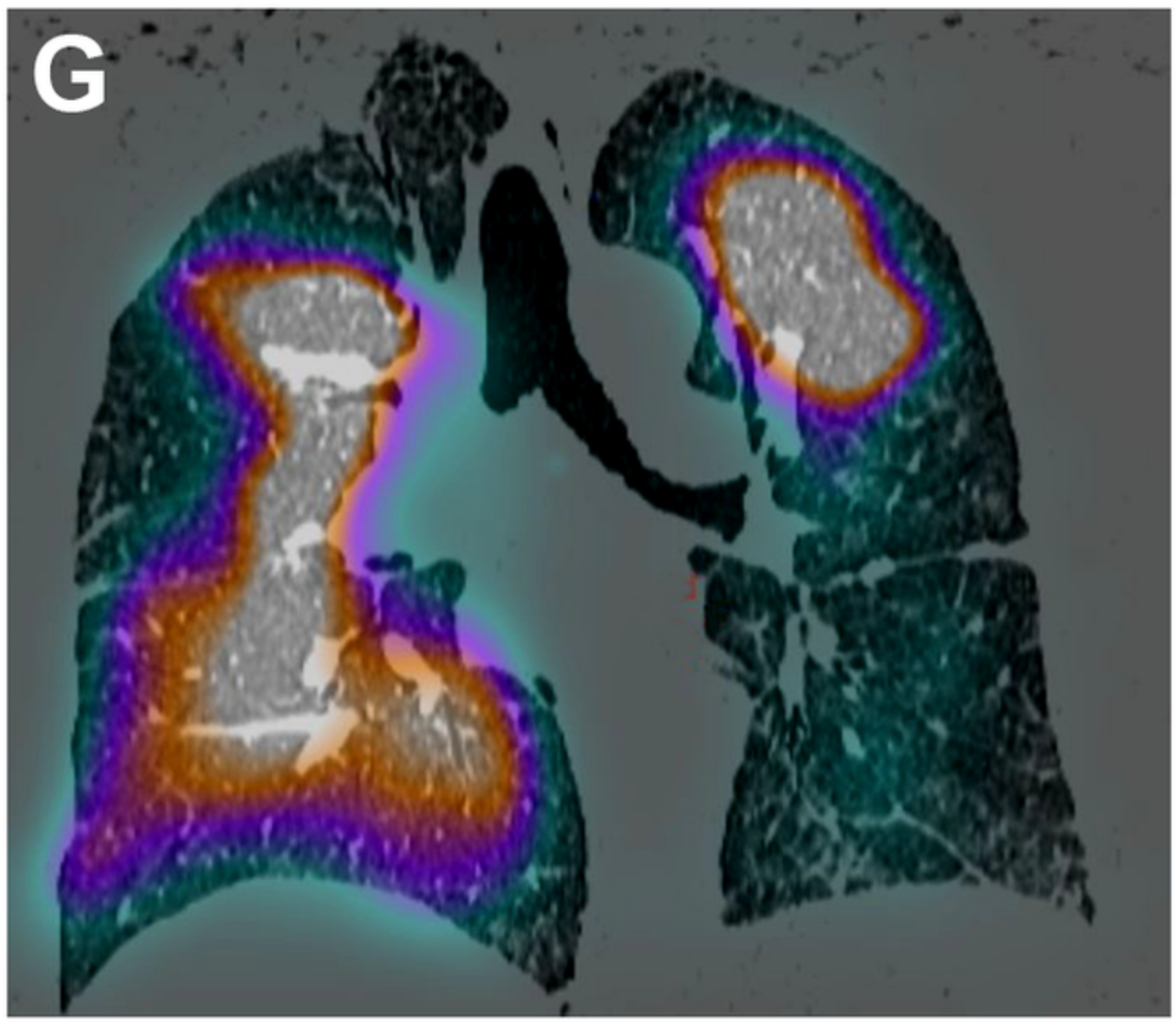
G

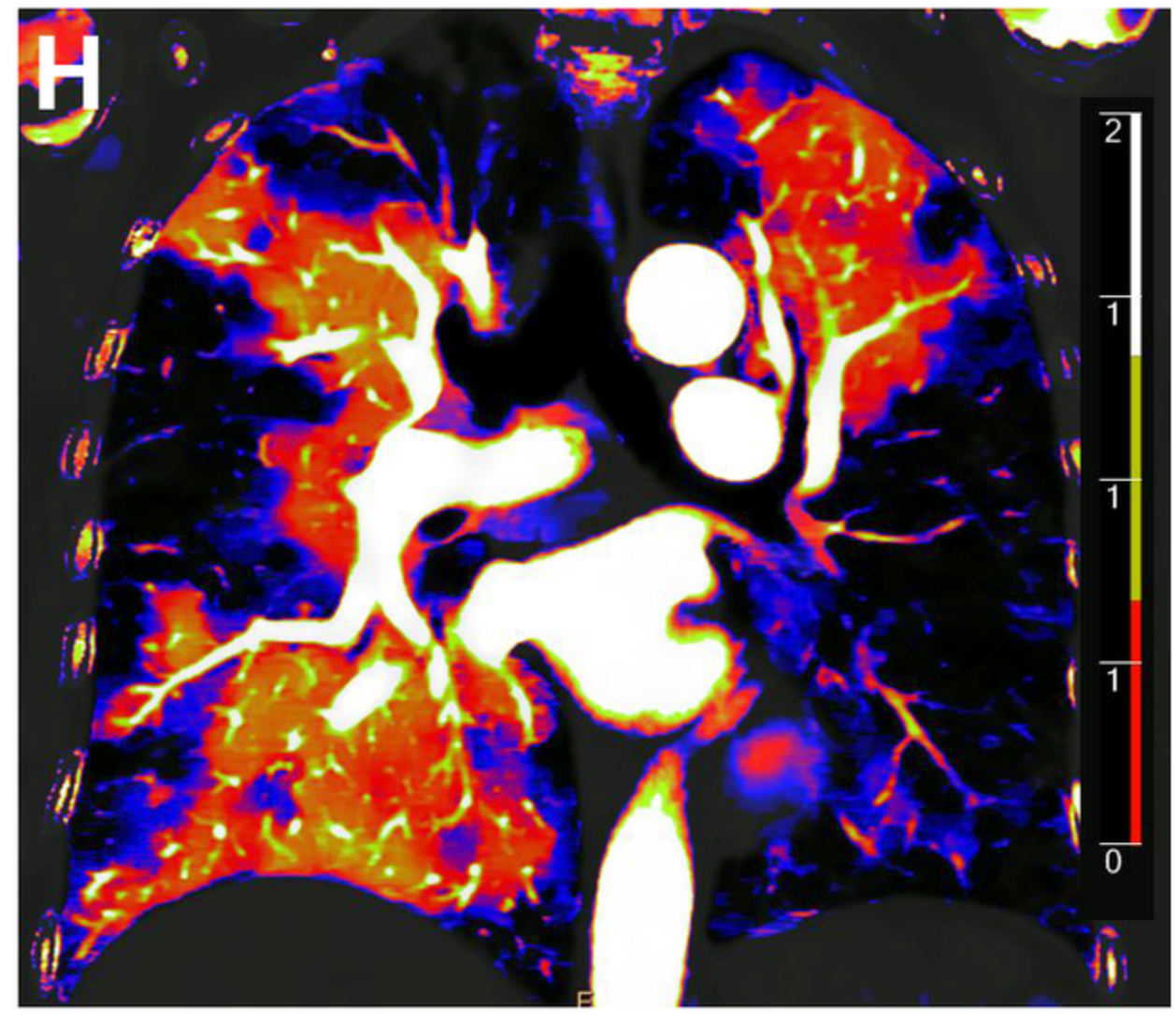
H
2
1
1
1
0

		DECT	SPECT	CT for SPECT fusion
Acquisition parameters				
	Tube voltage (kVp)	120	N.A.	120
	Collimation (mm)	64 ×0.65	N.A.	16 × 1.25
	Pitch	1.14 ± 0.08 [1.11-1.29]	N.A.	1.75
	Rotation time (sec)	0.31 ± 0.06 [0.27-0.33]	N.A.	0.5
	Tube current modulation	3D modulation		Longitudinal modulation
	Cranio-caudal acquisition	Yes	N.A.	Yes
	End-inspiratory acquisition	Yes	N.A.	Yes
	Iodine concentration (mg I/mL)	400	N.A.	N.A.
	Flow rate (mL/s)	3.5	N.A.	N.A.
	Volume or dose administered	20-30 mL (iodine) 20 mL (physiological saline solution)	Dose of 150 Mbq Tc 99m	N.A.
	Bolus tracking position	Pulmonary trunk	N.A.	N.A.
	Threshold (HU)	110	N.A.	N.A.
	Time of acquisition (sec)	2 - 3	15 s	10 - 12
Reconstruction parameters				
	Pixel size (mm)	0.68	4.37	0.80
	Matrice size	512	128	512
	Field of vue (mm)	350	560	410
	Lung images			
	Thickness (mm)	1	N.A.	1.25
	Intervals (mm)	0.7	N.A.	1
	Reconstruction algorithm	iDose^4 3	N.A.	ASiR 40%
	Kernel	Lung	N.A.	Lung
	Iodine images			
	Thickness (mm)	1	N.A.	N.A.
	Intervals (mm)	0.7	N.A.	N.A.
	Reconstruction algorithm	Spectral iDose^4 3	N.A.	N.A.
	Kernel	B (standard)	N.A.	N.A.

SPECT = scintigraphy photon emission computed tomography-computed tomography; ASIR = adaptive statistical iterative reconstruction; N.A. = not applicable; 3D = three-dimensional

Quantitative variables are expressed as means ± standard deviations (SD); numbes in brackets are ranges.

	Lobes	LUL	LLL	RUL	ML	RLL
Slope	0.89	0.73	0.78	0.74	0.73	0.75
Offset	2.12	6.86	5.91	5.71	1.09	5.06
R^2	0.87	0.85	0.81	0.81	0.70	0.87
RMSE	2.87	2.06	2.90	2.61	2.16	2.08
r	0.93	0.92	0.90	0.91	0.79	0.92
95% CI	0.92 - 0.95	0.87 - 0.95	0.83 - 0.94	0.85 - 0.95	0.66 - 0.87	0.86 - 0.95

LUL = left upper lobe; LLL = lower left lobe; RUL = right upper lobe; ML = middle lobe; RLL = right lower lobe); RMSE = root mean square error; 95% CI = 95% confidence interval